Article

Cell Reports

SAMHD1 Promotes DNA End Resection to Facilitate DNA Repair by Homologous Recombination

Graphical Abstract

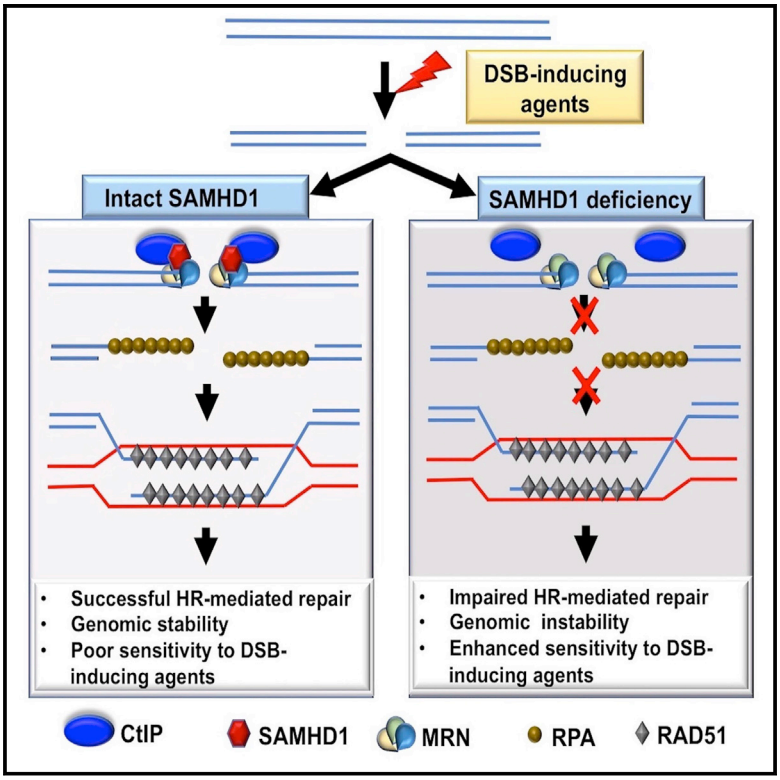

Highlights

- SAMHD1 deficiency or Vpx-mediated degradation sensitizes cells to DSB-inducing agents
- SAMHD1 localizes to DNA double-strand breaks in response to DNA damage
- SAMHD1 promotes HR and DNA end resection independent of its dNTPase activity
- SAMHD1 complexes with CtIP and facilitates its recruitment to DNA damage sites

Authors

Waaqo Daddacha, Allyson E. Koyen, Amanda J. Bastien, ..., Paul W. Doetsch, Baek Kim, David S. Yu

Correspondence

dsyu@emory.edu

In Brief

SAMHD1 is a dNTP triphosphohydrolase, which restricts HIV-1 infection and is dysregulated in Aicardi-Goutières syndrome and cancer. Daddacha et al. define a dNTPase-independent function for SAMHD1 in HR-mediated DSB repair by facilitating CtIP accrual to promote DNA end resection, providing insight into how SAMHD1 promotes genome integrity.

Accession Numbers

4BZB

Daddacha et al., 2017, Cell Reports *20*, 1921–1935
August 22, 2017
http://dx.doi.org/10.1016/j.celrep.2017.08.008

Cell Reports
Article

SAMHD1 Promotes DNA End Resection to Facilitate DNA Repair by Homologous Recombination

Waaqo Daddacha,[1,2] Allyson E. Koyen,[1,2] Amanda J. Bastien,[1,2] PamelaSara E. Head,[1,2] Vishal R. Dhere,[1,2] Geraldine N. Nabeta,[1,2] Erin C. Connolly,[1,2] Erica Werner,[1,2,3] Matthew Z. Madden,[1,2] Michele B. Daly,[4] Elizabeth V. Minten,[1,2] Donna R. Whelan,[5] Ashley J. Schlafstein,[1,2] Hui Zhang,[1,2] Roopesh Anand,[6] Christine Doronio,[1,2] Allison E. Withers,[1,2] Caitlin Shepard,[4] Ranjini K. Sundaram,[7] Xingming Deng,[1,2] William S. Dynan,[1,2,3] Ya Wang,[1,2] Ranjit S. Bindra,[7] Petr Cejka,[6] Eli Rothenberg,[5] Paul W. Doetsch,[1,2,3] Baek Kim,[4] and David S. Yu[1,2,8,*]

[1]Department of Radiation Oncology, Emory University School of Medicine, Atlanta, GA 30322, USA
[2]Winship Cancer Institute of Emory University, Atlanta, GA 30322, USA
[3]Department of Biochemistry, Emory University School of Medicine, Atlanta, GA 30322, USA
[4]Department of Pediatrics, Emory University School of Medicine, Atlanta, GA 30322, USA
[5]Department of Biochemistry and Molecular Pharmacology, NYU School of Medicine, New York, NY 10016, USA
[6]Institute for Research in Biomedicine, Università della Svizzera italiana, Via Vela 6, 6500 Bellinzona, Switzerland
[7]Department of Radiation Oncology, Yale University School of Medicine, New Haven, CT 06520, USA
[8]Lead Contact
*Correspondence: dsyu@emory.edu
http://dx.doi.org/10.1016/j.celrep.2017.08.008

SUMMARY

DNA double-strand break (DSB) repair by homologous recombination (HR) is initiated by CtIP/MRN-mediated DNA end resection to maintain genome integrity. SAMHD1 is a dNTP triphosphohydrolase, which restricts HIV-1 infection, and mutations are associated with Aicardi-Goutières syndrome and cancer. We show that SAMHD1 has a dNTPase-independent function in promoting DNA end resection to facilitate DSB repair by HR. SAMHD1 deficiency or Vpx-mediated degradation causes hypersensitivity to DSB-inducing agents, and SAMHD1 is recruited to DSBs. SAMHD1 complexes with CtIP via a conserved C-terminal domain and recruits CtIP to DSBs to facilitate end resection and HR. Significantly, a cancer-associated mutant with impaired CtIP interaction, but not dNTPase-inactive SAMHD1, fails to rescue the end resection impairment of SAMHD1 depletion. Our findings define a dNTPase-independent function for SAMHD1 in HR-mediated DSB repair by facilitating CtIP accrual to promote DNA end resection, providing insight into how SAMHD1 promotes genome integrity.

INTRODUCTION

DNA double-strand breaks (DSBs) are cytotoxic lesions induced by exogenous agents, such as ionizing radiation (IR), and endogenous sources, such as replication stress and meiotic recombination. Failure to repair DSBs leads to cell death or mutagenic events that drive genomic instability. Indeed, DSB repair defects are associated with cancer, premature aging, neurodegeneration, infertility, and developmental and immunological abnormalities (Jackson and Bartek, 2009). DSBs are repaired predominantly by two distinct, but highly coordinated pathways: error-prone non-homologous end joining (NHEJ), which involves direct ligation of broken DNA ends and error-free homologous recombination (HR), which involves an intact copy of the damaged site (Symington and Gautier, 2011). Whereas NHEJ operates throughout the cell cycle, HR functions primarily in S/G2 phase, when a sister chromatid is available as a repair template. HR is initiated by DNA end resection in which processing of the 5′ ends of DSBs by the CtBP-interacting protein (CtIP) endonuclease (Limbo et al., 2007; Makharashvili et al., 2014; Sartori et al., 2007; Wang et al., 2014; You et al., 2009), together with the MRE11-RAD50-NBS1 (MRN) endo and 3′ to 5′ exonuclease complex (Anand et al., 2016; Cannavo and Cejka, 2014; Garcia et al., 2011; Nicolette et al., 2010; Paull and Gellert, 1998; Stracker and Petrini, 2011), generates short 3′ single-stranded DNA (ssDNA) overhangs, which are further extended by the EXO1 or DNA2 nucleases together with the BLM or WRN helicase (Cejka et al., 2010; Gravel et al., 2008; Mimitou and Symington, 2008; Nimonkar et al., 2011; Niu et al., 2010; Zhu et al., 2008). The 3′ ssDNA overhangs are bound by RPA, which is then displaced by RAD51 to form a RAD51-ssDNA nucleoprotein filament with the assistance of mediator proteins, including BRCA2, to mediate HR (Prakash et al., 2015). RPA-ssDNA also recruits ATRIP to activate the ATR checkpoint kinase (Zhang et al., 2016; Zou and Elledge, 2003). Thus, DNA end resection is a critical determinant of DNA repair pathway choice and checkpoint activation.

Sterile alpha motif and histidine-aspartic acid (HD) domain-containing protein 1 (SAMHD1) is a deoxyribonucleoside triphosphate (dNTP) triphosphohydrolase (Goldstone et al., 2011; Powell et al., 2011) with a well-defined role in restricting HIV type 1 (HIV-1) and other viral infections, particularly in non-dividing cells by depleting dNTPs required for reverse transcription and replication (Baldauf et al., 2012; Hrecka et al., 2011; Laguette et al., 2011; Lahouassa et al., 2012). Mutations in SAMHD1 also cause Aicardi-Goutières syndrome (AGS) (Rice et al., 2009), a congenital neurodegenerative autoimmune disorder, and, moreover, SAMHD1 is recurrently mutated in chronic lymphocytic leukemia (CLL) (Clifford et al., 2014), frequently

mutated in colorectal cancer (Rentoft et al., 2016), as well as mutated or downregulated in a number of other cancers (Kohnken et al., 2015), suggesting that SAMHD1 functions as a tumor suppressor. SAMHD1 contains a SAM domain, a protein interaction module (Schultz et al., 1997) and a HD domain, found in a superfamily of proteins with metal-dependent phosphohydrolase activity (Aravind and Koonin, 1998). In addition to its well-established dNTPase activity, SAMHD1 binds to ssDNA/RNA (Beloglazova et al., 2013; Goncalves et al., 2012; Seamon et al., 2015, 2016; Tüngler et al., 2013) at its dimer-dimer interface, which sterically blocks tetramerization (Seamon et al., 2016) required for its dNTPase activity (Brandariz-Nuñez et al., 2013; Hansen et al., 2014; Ji et al., 2014; Yan et al., 2013; Zhu et al., 2013), and SAMHD1 has been reported to possess DNase/RNase activity (Beloglazova et al., 2013; Ryoo et al., 2014), however, a number of studies indicate that SAMHD1 lacks active-site-associated nuclease activity (Antonucci et al., 2016; Goldstone et al., 2011; Goncalves et al., 2012; Seamon et al., 2015, 2016; Welbourn and Strebel, 2016), which has been attributed to persistent co-purifying contaminants (Antonucci et al., 2016; Seamon et al., 2015).

SAMHD1 has been shown to promote genome integrity by maintaining dNTP pool balance through its dNTPase activity (Franzolin et al., 2013; Kohnken et al., 2015; Kretschmer et al., 2015; Clifford et al., 2014; Rentoft et al., 2016). Increased spontaneous DNA damage and dNTP pools was observed in cells from AGS patients with *SAMHD1* dysregulation (Kretschmer et al., 2015), and SAMHD1 depletion in cells leads to dNTP pool imbalance in cycling cells (Franzolin et al., 2013). Moreover, several heterozygous colorectal cancer-associated mutations impair SAMHD1's dNTPase activity, and elevated dNTP pools in combination with inactivated mismatch repair increase mutation rates, suggesting that heterozygous cancer-associated *SAMHD1* mutations increase mutation rates in cancer cells (Rentoft et al., 2016). Consistent with these findings, SAMHD1 overexpression in cells causes DNA damage hypersensitivity, however, somewhat paradoxical to its role in dNTP pool regulation, overexpressed SAMHD1-HA localizes to DNA damage sites (Clifford et al., 2014). How SAMHD1 functions to promote genome integrity is unclear. Here, we show that SAMHD1 has an unexpected dNTPase-independent function in promoting DNA end resection to facilitate DSB repair by HR through CtIP recruitment to DNA damage sites.

RESULTS

SAMHD1 Functions in DNA DSB Repair

To determine the role of SAMHD1 in responding to DNA damage, we examined U2OS cells depleted for SAMHD1 for sensitivity to IR, etoposide, and camptothecin (CPT), which directly or indirectly induce DSBs. Two small interfering RNAs (siRNAs) targeting SAMHD1 caused IR, CPT, and etoposide hypersensitivity compared to a non-targeting (NT) control (Figures 1A–1C), implying that SAMHD1 responds to DSBs. Western blot analysis confirmed SAMHD1 knockdown in these cells (Figure 1D). A similar CPT hypersensitivity following SAMHD1 depletion was observed in MCF7 cells, which could be rescued by expression of exogenous SAMHD1-GFP (Figures 1E and 1F), non-tumorigenic BEAS-2B cells, (Figures S1A and S1B), and was also observed in HCT-116 *SAMHD1* knockout (KO) cells (Figures S1C and S1D), suggesting that the phenotype is not cell-type specific, is not due to an off-target effect, and that SAMHD1-GFP is functional for alleviating DSB-inducing agent sensitivity. To provide direct evidence that SAMHD1 responds to DSBs at the single-cell level, we performed a neutral comet assay in U2OS cells depleted for SAMHD1 and treated with IR. SAMHD1 depletion in cells caused a significant delay in repair of IR-induced DSBs, as measured by comet tail moment compared to a NT control in cells synchronized in S phase (Figures 1G, 1H, and S1E), but not in unsynchronized cells (Figures S1E–S1G), suggesting that SAMHD1 promotes DSB repair predominantly in S phase, where HR is dominant.

SAMHD1 Localizes to DSBs in Response to DNA Damage

Overexpressed SAMHD1-HA has been reported to localize to DNA damage sites in response to CPT treatment (Clifford et al., 2014). To determine if endogenous SAMHD1 behaves similarly and localizes to DSBs, we analyzed SAMHD1 accumulation at DNA damage sites in response to IR and CPT treatment in HeLa cells. A significant increase in percent of cells with endogenous SAMHD1 foci was observed following IR and CPT treatment (Figure 2A), which co-localized with γH2AX, a marker for DSBs (Figure 2B), and RAD51, a marker for HR (Figure 2C), suggesting that SAMHD1 localizes directly to DSBs in response to DNA damage. Both endogenous SAMHD1 and SAMHD1-GFP expressed in U2OS cells also localized to DNA damage sites induced by laser microirradiation, which co-localized with RPA70, a marker for ssDNA formed by DSB end resection (Figures 2D and S2). To determine if endogenous SAMHD1 localizes to nascent DNA (naDNA) at CPT-induced one-sided DSBs and rule out co-localization resulting from random events, we used single-molecule super-resolution (SR) microscopy (Whelan et al., 2016) on U2OS cells pulse labeled with EdU and treated with or without CPT. Similar to CtIP, a significant increase in co-localization of SAMHD1 with naDNA above random levels was observed following CPT treatment (Figures 2E and 2F), suggesting that SAMHD1 localizes directly to replication-associated DSBs.

SAMHD1 Functions in DSB Repair by Facilitating HR

Poly ADP-ribose polymerase (PARP) inhibitor sensitivity is associated with defects in HR (Helleday et al., 2005). Indeed, SAMHD1 depletion in U2OS, MCF7, and primary small airway epithelial cells caused hypersensitivity to veliparib, a PARP inhibitor (Figures 3A, 3B, and S3A–S3C), which could be rescued with expression of exogenous SAMHD1-GFP (Figure 3B), suggesting that SAMHD1 may function in HR. To more directly determine if SAMHD1 functions in HR, we examined SAMHD1 depletion in U2OS cells integrated with a direct repeat (DR)-GFP reporter substrate in which expression of I-SceI endonuclease generates a DSB that when repaired by HR restores GFP expression (Pierce et al., 1999). SAMHD1 depletion caused an impairment in HR (Figure 3C), suggesting directly that SAMHD1 functions in HR. Notably, while SAMHD1 depletion in U2OS cells resulted

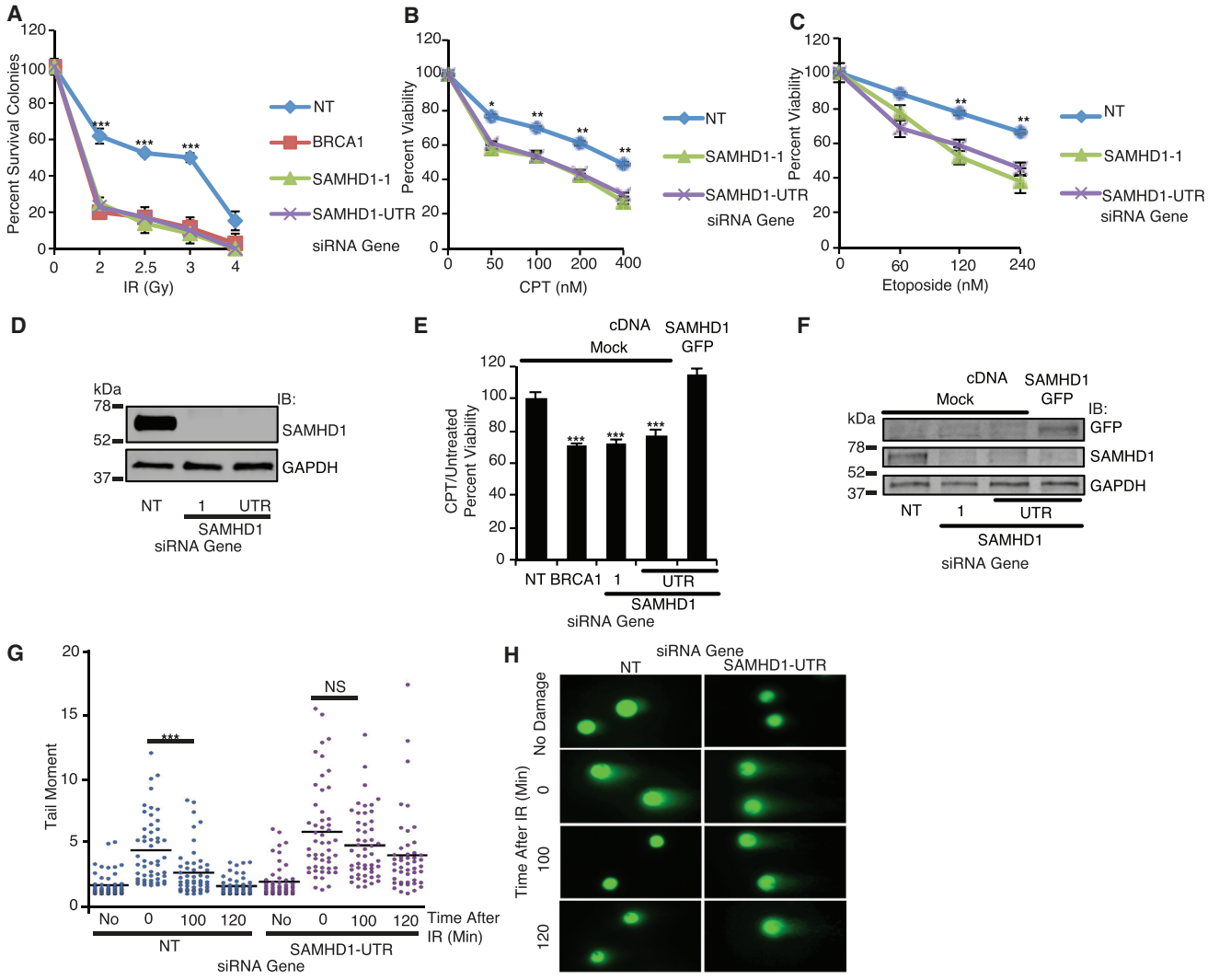

Figure 1. SAMHD1 Functions in DNA DSB Repair

(A) U2OS cells transfected with indicated siRNA were seeded for colony formation, treated with indicated doses of IR, and assayed for surviving colonies 12 days later. The percent of surviving colonies is shown.

(B and C) U2OS cells transfected with non-targeting (NT) or SAMHD1 siRNA were treated with indicated doses of CPT (B) or etoposide (C) for 72 hr and assayed for cell viability using Alamar Blue.

(D) Western blot analysis showing SAMHD1 knockdown in U2OS cells at 72 hr.

(E) MCF7 cells transfected with indicated siRNAs and plasmids were treated with 200 nM CPT for 72 hr and assayed for viability with Alamar Blue. The treated to untreated viability relative to NT siRNA is shown.

(F) Western blot analysis in MCF7 cells demonstrating SAMHD1 knockdown and expression of SAMHD1-GFP.

(G and H) U2OS cells transfected with indicated siRNAs were synchronized by mimosine arrest for 16 hr, released into S phase, and exposed to 10 Gy IR (G). DNA damage was analyzed by neutral comet assay (H).

(G) Dot plot with median of comet tail moment is shown.

(H) Representative images of comet tails are shown.

(A–C, E, and G) Mean and SEM from at least three independent replicas are shown. *$p < 0.05$, **$p < 0.01$, and ***$p < 0.001$. See also Figure S1.

in a 1.5- to 3-fold increase in dNTP pool concentration (Figures S3D and S3E), we did not observe any significant change in cell cycle (Figures 3D and 3E), suggesting that the observed effect is not due to an indirect effect of cell cycle change. Consistent with this finding, SAMHD1 depletion in HeLa cells and non-tumorigenic BEAS-2B cells impaired RAD51, but not γH2AX foci accumulation in response to CPT and IR treatment (Figures 3F–3H, S3F, and S3G), indicating that SAMHD1 is required for HR, but not for DSB induction by CPT. In contrast, SAMHD1 depletion in U2OS cells transfected with the pEGFP-Pem1-Ad2 NHEJ reporter substrate (Seluanov et al., 2004) caused no significant impairment in NHEJ and only a mild increase in NHEJ with one siRNA (Figures S3H and S3I), implying that SAMHD1 specifically promotes HR, but not NHEJ in DSB repair.

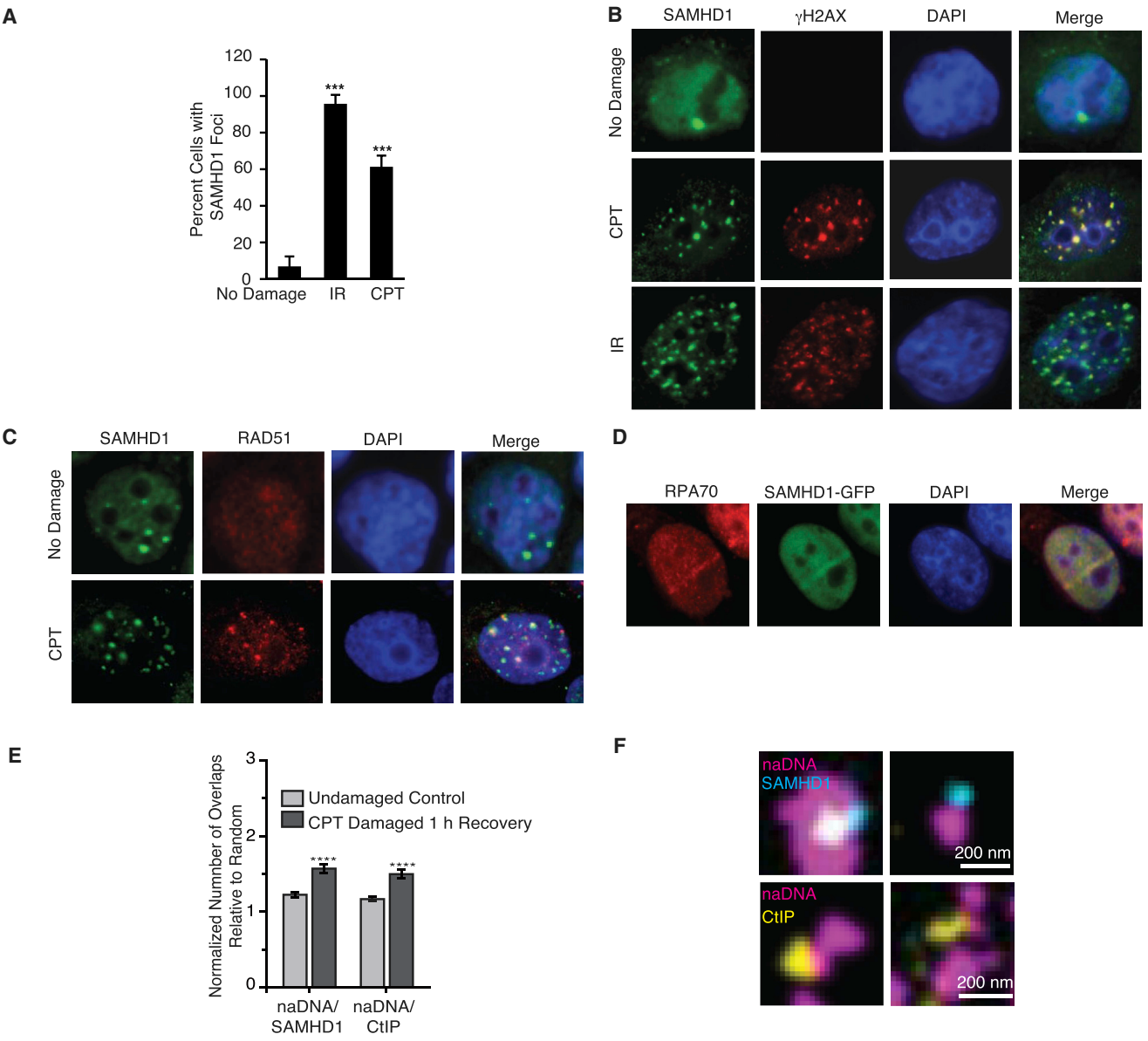

Figure 2. SAMHD1 Localizes to DSBs in Response to DNA Damage

(A–C) HeLa cells were treated with 2 μM CPT for 4 hr, fixed, and processed for immunofluorescence with indicated antibodies.

(A) Percent cells with SAMHD1 foci are shown.

(B and C) Representative immunofluorescence images of SAMHD1 co-localizing with γH2AX (B) or RAD51 (C) after DNA damage are shown.

(D) U2OS cells expressing SAMHD1-GFP were microirradiated, fixed after 1 min, and processed for immunofluorescence with anti-RPA70 antibodies.

(E and F) U2OS cells were treated with 0.1 μM CPT and 10 μM EdU for 1 hr, washed, and processed 1 hr for immunofluorescence with click chemistry and anti-SAMHD1 and CtIP antibodies. Quantitation (E) and representative SR images (F) of co-localization between nascent DNA (naDNA via EdU) and SAMHD1 or CtIP showing increased association upon CPT damage are shown.

(A and E) Mean and SEM from at least three independent replicas are shown. ***$p < 0.001$ and ****$p < 0.0001$. See also Figure S2.

SAMHD1 Facilitates HR and ATR Activation by Promoting DNA End Resection

HR is initiated by DNA end resection. Thus, we examined for RPA32 phosphorylation at Ser4/8, a marker for DNA end resection following CPT treatment. SAMHD1 depletion in U2OS cells impaired RPA32 Ser4/8 phosphorylation, but not total RPA32 levels in response to CPT (Figure 4A). Consistent with these findings, SAMHD1 depletion and KO in U2OS, BEAS-2B, and primary small airway epithelial cells caused a significant decrease in RPA70 foci formation in response to CPT and IR (Figures 4B, 4C, S4A–S4D, and S4F–S4I) and moreover impaired GFP-RPA70 recruitment to DNA damage sites induced by laser microirradiation (Figures 4D and S4E). ATRIP localization to DNA damage sites is dependent on its interaction with RPA-ssDNA. In

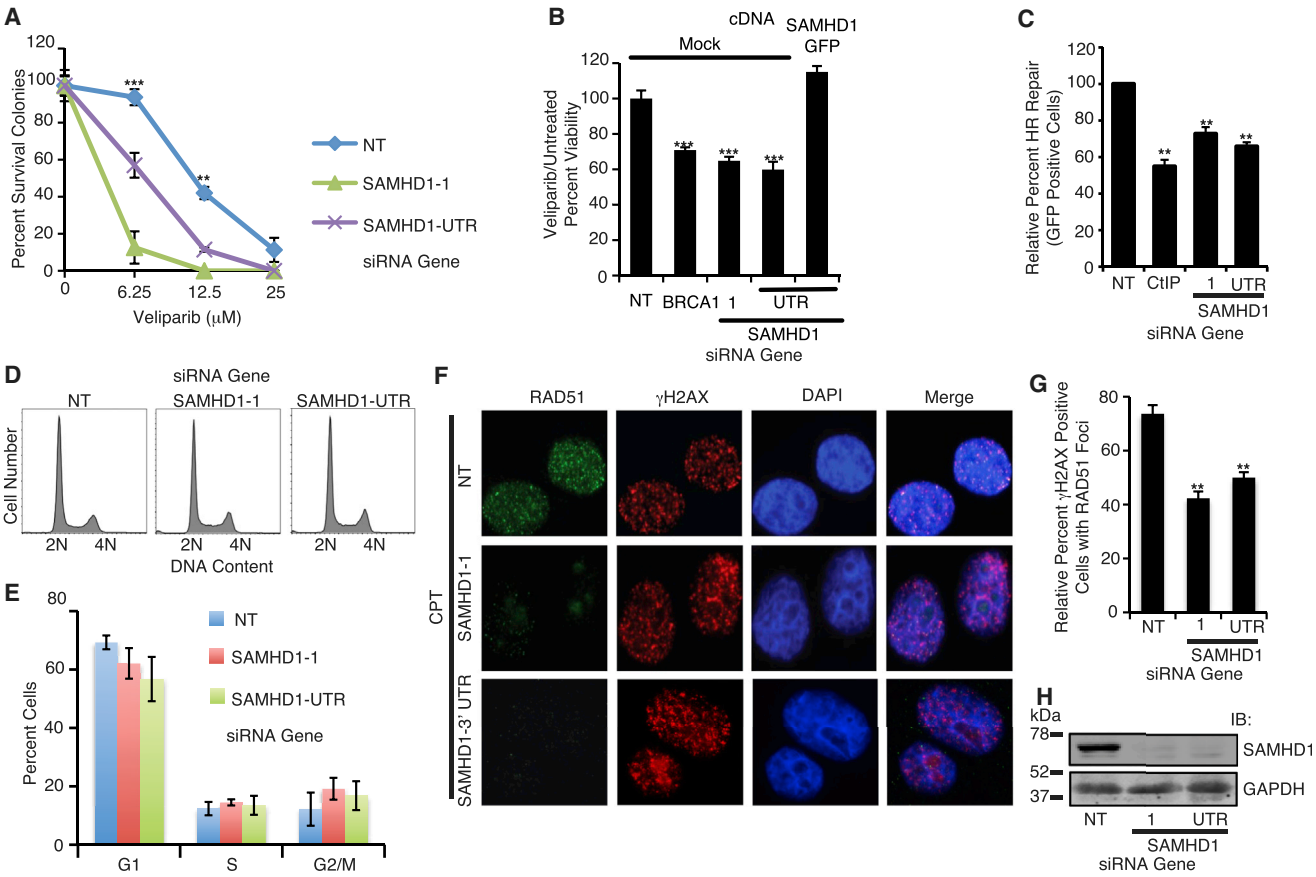

Figure 3. SAMHD1 Functions in DSB Repair by Facilitating HR

(A) U2OS cells transfected with NT or SAMHD1 siRNA were treated with indicated doses of veliparib and assayed for surviving colonies 12 days later. The percent of surviving colonies is shown.

(B) MCF7 cells transfected with indicated siRNAs and plasmids were treated with 50 μM veliparib for 72 hr and assayed for viability with Alamar Blue. The treated to untreated viability relative to NT siRNA is shown.

(C) U2OS cells integrated with a DR-GFP HR reporter substrate were transfected with indicated siRNAs and I-SceI, fixed, and analyzed for HR by GFP expression using flow cytometry.

(D) Cell cycle profile of U2OS cells depleted for SAMHD1 was determined by flow cytometry.

(E) Quantitation of cell cycle profile shown.

(F and G) HeLa cells transfected with SAMHD1 or NT siRNA were treated with 2 μM CPT for 4 hr, fixed, and processed for immunofluorescence with indicated antibodies. Representative images (F) and quantitation (G) of relative percent γH2AX-positive cells with RAD51 foci are shown.

(H) Western blot analysis showing SAMHD1 knockdown in HeLa cells at 72 hr.

(A–C, E, and G) Mean and SEM from at least three replicas are shown. **$p < 0.01$ and ***$p < 0.001$. See also Figure S3.

this regard, SAMHD1 depletion in cells also impaired GFP-ATRIP foci accumulation in response to CPT (Figures 4E and 4F). Moreover, SAMHD1 depletion in cells impaired CPT-induced ATR autophosphorylation at Thr-1989, but not total ATR levels (Figure 4G), suggesting that SAMHD1 is required for efficient ATR activation following CPT treatment. To more directly determine the role of SAMHD1 in DNA end resection, we labeled U2OS cells with BrdU, treated the cells with CPT, and probed the cells for BrdU exposure under non-denaturing conditions, which labels ssDNA. SAMHD1 depletion also impaired BrdU foci under these conditions (Figures 4H and 4I), providing direct support for SAMHD1 in promoting DNA end resection. Importantly, given its role as a dNTPase, SAMHD1 depletion in these cells caused only a mild, but insignificant, impairment in BrdU incorporation under denaturing conditions (Figure S4J) and to a much lesser extent than impairment in CPT-induced BrdU foci (cf. Figure 4I). Taken together, these data strongly suggest that SAMHD1 facilitates HR and ATR activation by promoting DNA end resection.

SAMHD1 Promotes HR and DNA End Resection Independent of Its dNTPase Activity

SAMHD1 has been proposed to maintain genome integrity by regulating dNTP pools. To determine if SAMHD1 dNTPase activity is required for DSB repair, we performed rescue experiments with SAMHD1-RFP H206A/D207A, which disrupts SAMHD1's active site and impairs its dNTPase activity (Goldstone et al., 2011; Laguette et al., 2011) and reported DNase/RNase activities (Beloglazova et al., 2013). Both SAMHD1-RFP wild-type

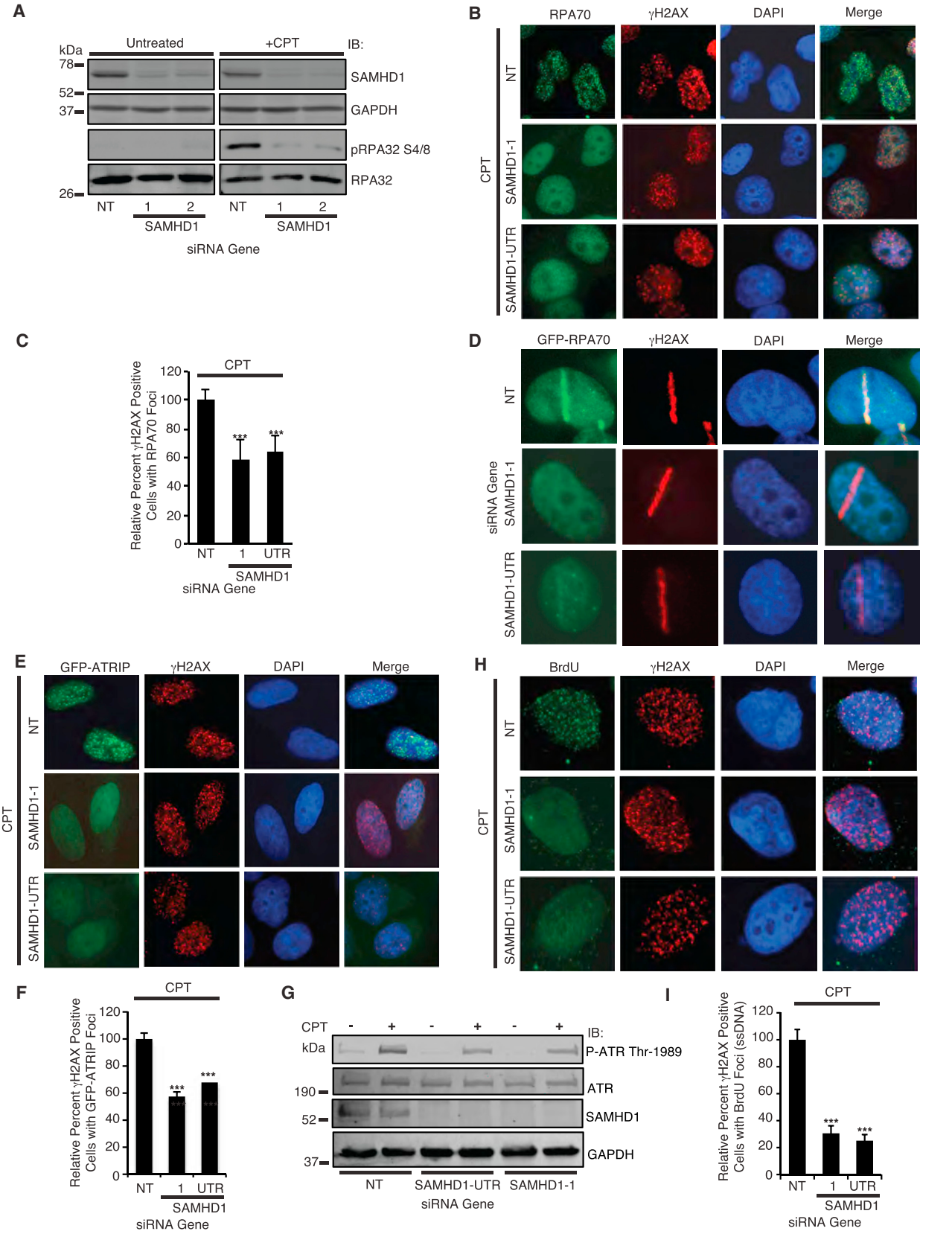

(legend on next page)

(WT) and H206A/D207A restored the HR impairment of SAMHD1 depletion in U2OS cells (Figures 5A, 5B, and S5A), suggesting that SAMHD1's role in promoting HR is independent of its dNTPase activity. SAMHD1-HA WT and H206A/D207A also alleviated the IR-induced RPA70 foci impairment of SAMHD1 depletion in U2OS cells (Figure 5C), suggesting that SAMHD1 promotes DNA end resection independent of its dNTPase activity.

SAMHD1 Interacts in a Complex with CtIP in Response to DNA Damage

Because our findings suggest that SAMHD1 facilitates HR by promoting DNA end resection and its role in HR is independent of its active-site catalytic activity, we determined whether SAMHD1 might function with other nucleases. Co-immunoprecipitation (coIP) of SAMHD1-HA expressed in 293T cells pulled down GFP-CtIP and endogenous MRE11 (Figure 5D), and, similarly, coIP of CtIP-FLAG pulled down SAMHD1-RFP in response to IR (Figure 5E), suggesting that SAMHD1 interacts with CtIP and MRE11 in a damage-regulated manner. We validated that endogenous SAMHD1 coIPs with endogenous CtIP in response to IR (Figure 5F), and that endogenous SAMHD1 coIPs with GFP-MRE11 in response to IR (Figure S5B). The coIP of endogenous SAMHD1 with CtIP and MRE11 following IR was preserved even following benzonase nuclease treatment (Figure S5C), suggesting that the damage-regulated interaction of SAMHD1 with CtIP and MRE11 is not mediated through DNA. Moreover, bacterially recombinant SAMHD1 pulled down recombinant GST-CtIP (Figure 5G), suggesting that SAMHD1 binds directly to CtIP. To identify the region of SAMHD1 that interacts with CtIP, we generated SAMHD1 deletion mutants and performed coIP of SAMHD1 WT and mutants with GFP-CtIP expressed in 293T cells. In contrast to SAMHD1-HA (1–115), SAMHD1-HA (115–562) coIP'd with GFP-CtIP (Figures 5H and 5J), suggesting that the HD, but not SAM, domain region of SAMHD1 is sufficient for CtIP interaction. In further mapping experiments, SAMHD1-HA (1–562), but not SAMHD1 (1–465), coIP'd with GFP-CtIP expressed in 293T cells (Figures 5I and 5J), suggesting that SAMHD1 amino acids (aa) 465–562 are necessary for interaction with CtIP. To provide insight into the binding surface of the CtIP interaction domain of SAMHD1, we examined the crystal structure of tetrameric SAMHD1 (Ji et al., 2013) and observed that aa 465–562 are located on the surface of tetrameric SAMHD1 (Figure S5D). Interestingly, a naturally occurring cancer-associated *SAMHD1* mutation (K484T) from a patient with gastric cancer reported in The Cancer Genome Atlas (TCGA) through the cBioPortal for Cancer Genomics (Cerami et al., 2012) is located in this region facing the outside of tetrameric SAMHD1 (Figure S5D) and is evolutionarily conserved (Figure 5J). While SAMHD1-GFP K484T overexpressed in cells showed no significant impairment in dNTPase activity compared with SAMHD1-GFP WT (Figures S5E and S5F), SAMHD1-HA K484T showed an impairment in coIP with GFP-CtIP compared with SAMHD1-HA WT (Figure 5K), suggesting that K484 is critical for SAMHD1's interaction with CtIP, but not dNTPase activity, and that a cancer-associated *SAMHD1* mutation is functionally significant in impairing the interaction of SAMHD1 with CtIP.

SAMHD1 Recruits CtIP to DNA Damage Sites and Chromatin in Response to DNA Damage and Promotes DNA End Resection through Its Interaction with CtIP

The damage-regulated interaction of SAMHD1 and CtIP suggests that they may function together to promote DNA end resection. Consistent with this finding, a significant increase in co-localization of SAMHD1 with CtIP was observed following CPT treatment (Figures 6A and 6B). To determine if SAMHD1 cooperates with CtIP in promoting HR and DNA end resection, we performed epistasis experiments using the DR-GFP reporter assay and CPT-induced RPA70 foci as readouts. Combined depletion of SAMHD1 and CtIP did not result in a significantly greater HR defect or CPT-induced RPA70 foci impairment compared with their depletion alone (Figures 6C and 6D), suggesting that SAMDH1 cooperates with CtIP in promoting DNA end resection to facilitate DSB repair by HR. To determine if SAMHD1 functions upstream of CtIP or MRE11, we evaluated the recruitment of GFP-CtIP and GFP-MRE11 to DNA damage sites. SAMHD1 depletion and KO in U2OS cells impaired GFP-CtIP, but not GFP-MRE11 or γH2AX localization to DNA damage sites induced by laser microirradiation (Figures 6E and S6), suggesting that SAMHD1 facilitates CtIP, but not MRE11, recruitment to DNA DSBs. Consistent with these findings, SAMHD1 depletion in HCT-116 cells impaired the mobilization of endogenous CtIP to chromatin in response to IR (Figure 6F). To determine if SAMHD1's interaction with CtIP is required for its role in DNA end resection, we performed rescue experiments with SAMHD1 K484T. In contrast to SAMHD1 H206A/D207A, which is proficient in HR and DNA end resection (Figures 5A and 5C), SAMHD1-RFP/GFP K484T failed to rescue the damage-induced

Figure 4. SAMHD1 Facilitates HR and ATR Activation by Promoting DNA End Resection

(A) U2OS cells transfected with SAMHD1 or NT siRNA were treated with 2 μM CPT for 4 hr, harvested, run on SDS-PAGE, and probed with indicated antibodies.

(B and C) U2OS cells transfected with SAMHD1 or NT siRNA were treated with 2 μM CPT for 4 hr, fixed, and processed for immunofluorescence with indicated antibodies. Representative images (B) and quantitation (C) of relative percent γH2AX-positive cells with RPA70 foci are shown.

(D) Representative images of GFP-RPA70-expressing U2OS cells transfected with NT or SAMHD1 siRNA, subjected to laser microirradiation, fixed 5 min after damage, and processed for immunofluorescence with anti-γH2AX antibodies.

(E and F) U2OS cells stably transfected with GFP-ATRIP were treated with 2 μM CPT for 4 hr, fixed, and processed for immunofluorescence with anti-γH2AX antibodies. Representative images (E) and quantitation (F) of relative percent γH2AX-positive cells with GFP-ATRIP foci are shown.

(G) HCT-116 cells transfected with SAMHD1 or NT siRNA were treated with 2 μM CPT for 4 hr, harvested, run on SDS-PAGE, and probed with indicated antibodies.

(H and I) SAMHD1 depleted U2OS cells were treated with 30 μM BrdU for 36 hr, followed by 3 μM CPT treatment for 4 hr. Cells were fixed under non-denaturing conditions and processed for immunofluorescence using anti-BrdU (ssDNA) and γH2AX antibodies. Representative images (H) and quantitation (I) of relative percent γH2AX-positive cells with BrdU foci are shown.

(C, F, and I) Mean and SEM from three independent replicas are shown. ***$p < 0.001$. See also Figure S4.

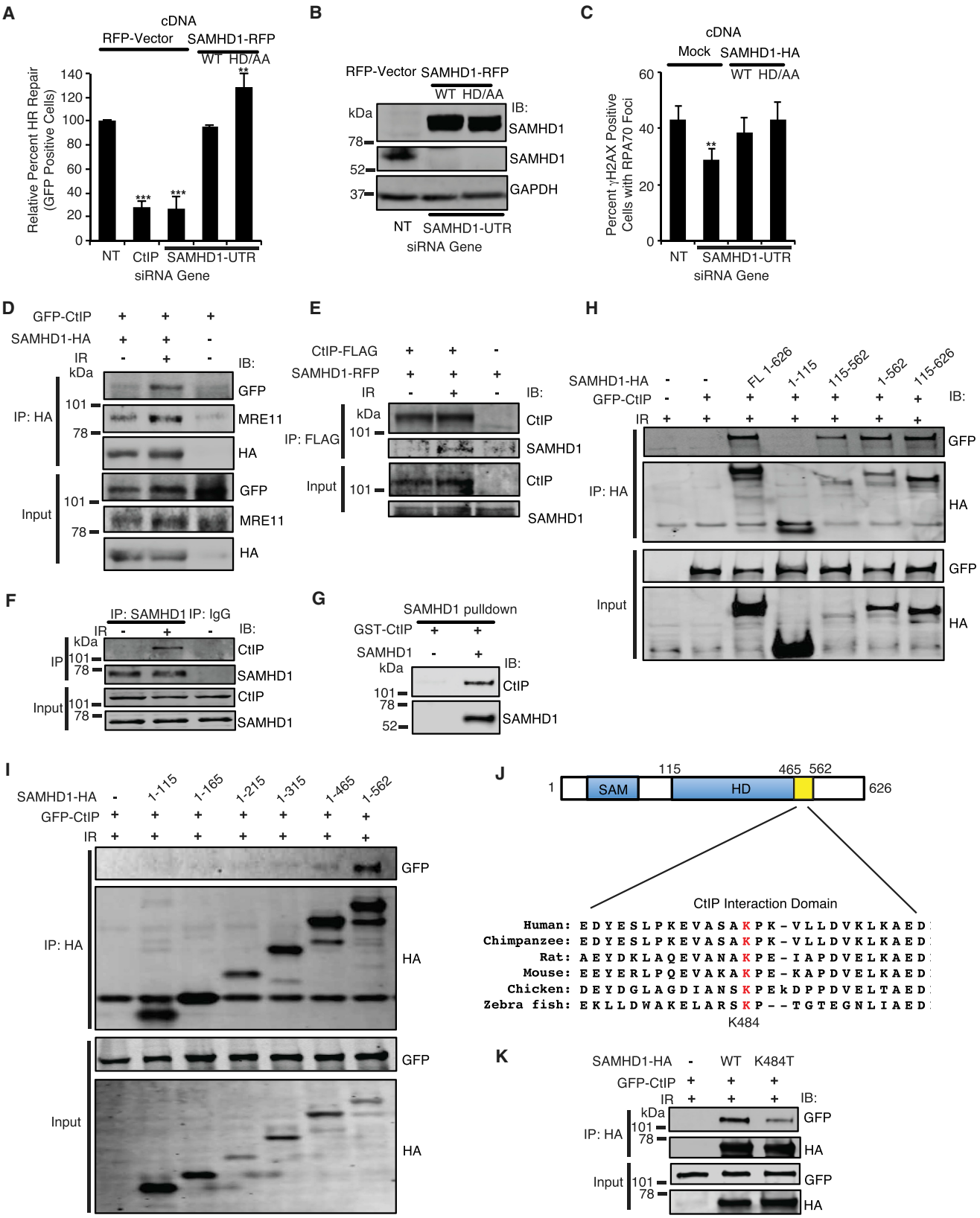

(legend on next page)

CtIP recruitment, IR-induced RPA70 foci impairment, and CPT hypersensitivity of SAMHD1 deficiency in U2OS cells (Figures 6G–6J), suggesting that SAMHD1 promotes DNA end resection through its interaction with CtIP, and that this is impaired by a naturally occurring cancer-associated *SAMHD1* mutation. Collectively, these results imply that SAMHD1 recruits CtIP to DSBs to facilitate DNA end resection and HR.

Targeting SAMHD1 with Virus-like Particles Containing Vpx Sensitizes Cancer Cells to DSB-Inducing Agents

SAMHD1 is targeted for proteasomal degradation by the retrovirus accessory protein Vpx (Hrecka et al., 2011; Laguette et al., 2011), and virus-like particles (VLPs) containing Vpx have been used to sensitize acute myelogenous leukemia cells to cytarabine chemotherapy (Herold et al., 2017; Hollenbaugh et al., 2017; Schneider et al., 2017). U2OS cells treated with VLPs containing Vpx showed reduced SAMHD1 protein levels compared with cells treated with VLPs containing no Vpx (Figure 7A). Similar to cancer cells with SAMHD1 deficiency by genetic knockdown or KO, U2OS cells treated with VLPs containing Vpx showed hypersensitivity to CPT and veliparib compared to control cells (Figures 7B and 7C). Moreover, the CPT hypersensitivity of U2OS cells treated with VLPs containing Vpx was alleviated by overexpression of SAMHD1-GFP (Figures 7D and 7E), implying that the effects are mediated specifically through SAMHD1 degradation. Collectively, these data suggest that targeting SAMHD1 with VLPs containing Vpx sensitizes cancer cells to DSB-inducing agents and may be a promising therapeutic strategy for cancer treatment.

DISCUSSION

Our findings reveal a dNTPase-independent function for SAMHD1 in promoting HR-mediated DSB repair by facilitating DNA end resection through CtIP accrual, demonstrating that SAMHD1 has a direct role in genome maintenance independent of its role in dNTP pool regulation, establishing SAMHD1 as a critical regulator of DNA end resection in promoting DSB repair by HR and identifying the CtIP/MRE11 nucleases as unique interacting partners for SAMHD1. In this regard, we found that SAMHD1 deficiency by genetic knockdown or KO or proteasomal degradation by VLPs containing Vpx in cells causes IR, CPT, and etoposide hypersensitivity, and SAMHD1 is recruited to DSBs that co-localize with γH2AX, RAD51, RPA70, and naDNA in response to DNA damage. SAMHD1 depletion further causes PARP inhibitor sensitivity, impaired RAD51 recruitment to foci, and impaired HR, but not NHEJ, through direct reporter assays. Moreover, SAMHD1 depletion impairs BrdU exposure, RPA Ser4/8 phosphorylation, and RPA recruitment to DSBs, suggesting that SAMDH1 facilitates DNA end resection. SAMHD1 depletion also impairs CPT-induced ATRIP foci accumulation and ATR autophosphorylation, suggesting that SAMHD1 is required for efficient ATR activation following CPT treatment. Mechanistically, SAMHD1 interacts directly with CtIP via an evolutionarily conserved domain in its C terminus, which is disrupted by a naturally occurring cancer-associated *SAMHD1* mutation, and MRE11 in a damage-regulated manner, and is required for CtIP, but not MRE11, recruitment to DNA damage sites. In contrast to dNTPase-inactive SAMHD1, which is proficient for HR and DNA end resection, the cancer-associated SAMHD1 mutant with impaired CtIP interaction and proficient dNTPase activity fails to rescue the damage-induced CtIP recruitment deficit, IR-induced RPA70 foci impairment, and CPT hypersensitivity of SAMHD1 deficiency. Thus, our findings support a model in which SAMHD1 promotes DSB repair by HR independent of its well-established dNTPase activity by facilitating CtIP recruitment, which in turn cooperates with MRN to promote DNA end resection (Figure 7F).

SAMHD1 has been reported to possess nuclease activity (Beloglazova et al., 2013; Ryoo et al., 2014), which has since been attributed to persistent co-purifying contaminants (Antonucci et al., 2016; Seamon et al., 2015). Our finding of a rescue of the HR and DNA end resection impairment of SAMHD1 depletion with an active-site mutant of SAMHD1, which abolishes its dNTPase activity and reported nuclease activity, and interaction of SAMHD1 with CtIP/MRE11, which are known nucleases,

Figure 5. SAMHD1 Promotes HR and DNA End Resection Independent of Its dNTPase Activity and Complexes with CtIP in Response to DNA Damage

(A) U2OS cells integrated with a DR-GFP HR reporter substrate were transfected with indicated siRNAs, cDNAs, and I-SceI and fixed. RFP-positive cells were gated and analyzed for HR by GFP expression using flow cytometry.

(B) Western blot analysis in U2OS cells demonstrating SAMHD1 knockdown and expression of SAMHD1-RFP.

(C) U2OS cells were transfected with indicated siRNAs and cDNA, treated with 10 Gy IR, and processed 4 hr later for immunofluorescence with indicated antibodies. Quantitation of percent γH2AX-positive cells with RPA70 foci that are HA-SAMHD1 positive for complemented cells is shown.

(D) 293T cells were transfected with GFP-CtIP and SAMHD1-HA, treated with 10 Gy IR, harvested 4 hr later, IP'd with anti-HA antibodies, run on SDS-PAGE, and immunoblotted with indicated antibodies.

(E) 293T cells were transfected with CtIP-FLAG and SAMHD1-RFP, treated with 10 Gy IR, harvested 4 hr later, IP'd with anti-FLAG antibodies, run on SDS-PAGE, and immunoblotted with indicated antibodies.

(F) Endogenous SAMHD1 was IP'd from lysate from HCT-116 cells treated with or without IR, washed, separated by SDS-PAGE, and immunoblotted with indicated antibodies.

(G) Recombinant GST-CtIP and SAMHD1 purified from *E. coli* was pulled down with an anti-SAMHD1 antibody, washed, separated by SDS-PAGE, and immunoblotted with indicated antibodies.

(H and I) 293T cells were transfected with full-length or truncated SAMHD1-HA WT and GFP-CtIP, treated with 10 Gy, IR, harvested 4 hr later, IP'd with anti-HA antibodies, run on SDS-PAGE, and immunoblotted with indicated antibodies. Domain mapping analysis indicates that aa 115–562 are sufficient for interaction with CtIP (H) and aa 465–562 are necessary for interaction with CtIP (I).

(J) Schematic representation of SAMHD1 structural domains and evolutionary conservation of CtIP interaction domain.

(K) A naturally occurring cancer-associated *SAMHD1* mutation (K484T) impairs the interaction of SAMHD1 with CtIP.

(A and C) Mean and SEM from three independent replicas are shown. $^{**}p < 0.01$ and $^{***}p < 0.001$. See also Figure S5.

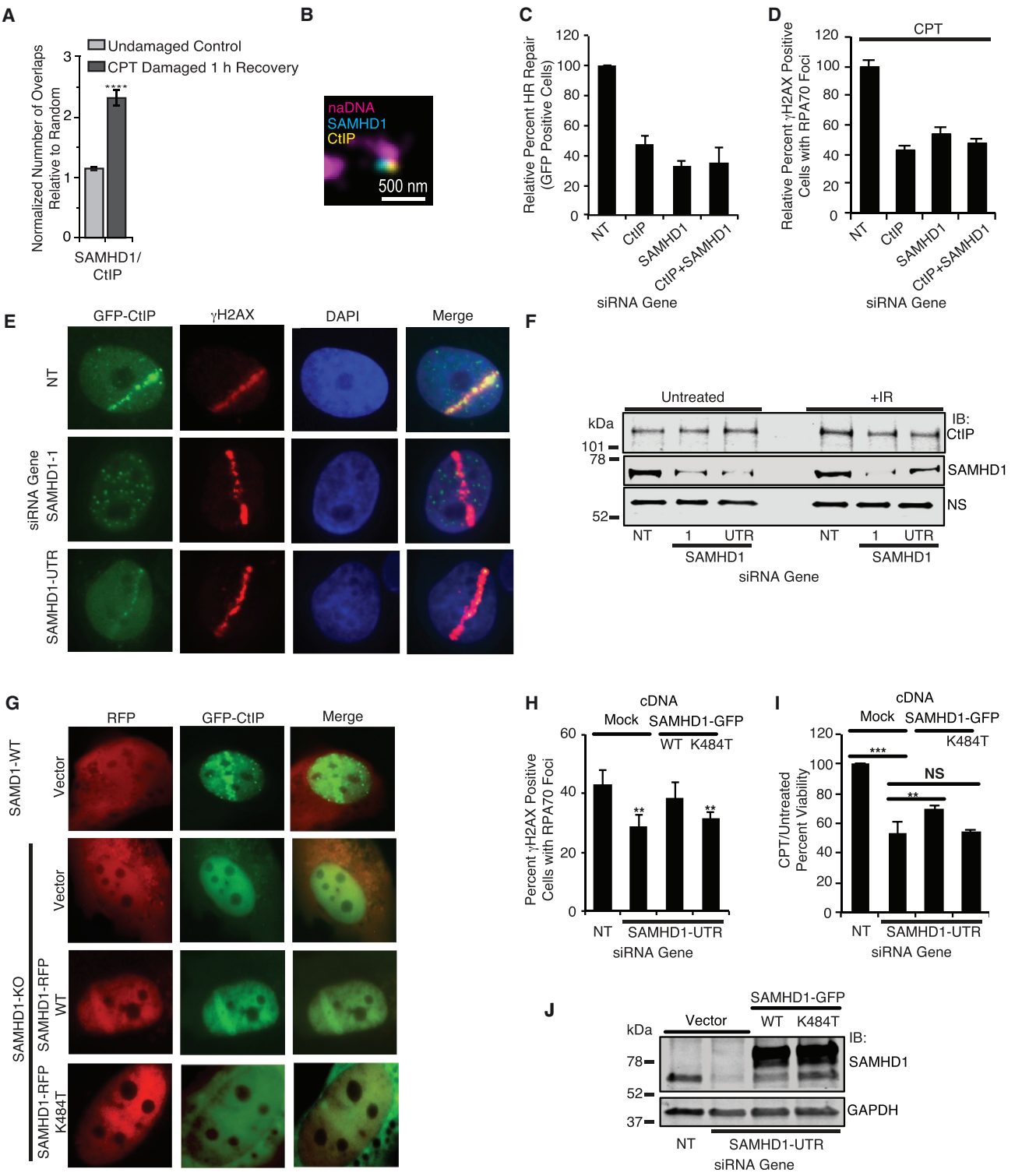

Figure 6. SAMHD1 Recruits CtIP to DNA Damage Sites and Chromatin in Response to DNA Damage and Promotes DNA End Resection through Its Interaction with CtIP

(A and B) U2OS cells were treated with 0.1 μM CPT and 10 μM EdU for 1 hr, washed, and processed 1 hr for immunofluorescence with click chemistry and anti-SAMHD1 and CtIP antibodies.

(A) Quantitation of co-localization of SAMHD1 and CtIP upon CPT damage.

(legend continued on next page)

suggest that SAMHD1's role in promoting DNA end resection is likely independent of any intrinsic catalytic activity and thus through a scaffold function. In this respect, SAMHD1 localizes to naDNA at CPT-induced DSBs and binds to ssDNA/RNA (Beloglazova et al., 2013; Goncalves et al., 2012; Seamon et al., 2015, 2016; Tüngler et al., 2013) and could facilitate CtIP recruitment to or stabilization at DSBs through this interaction. CtIP recruitment to DNA damage sites is also dependent on its interaction with the MRN complex (You et al., 2009; Yuan and Chen, 2009), BRCA1 (Yu et al., 2006), and its own tetramerization (Wang et al., 2012), which could be regulated by SAMHD1.

Given SAMHD1's well-established role as a dNTPase, how might this activity be reconciled with its role in promoting DNA end resection and HR? SAMHD1 binds to ssDNA at its dimer-dimer interface, which sterically blocks its tetramerization into its dNTPase active form (Brandariz-Nuñez et al., 2013; Hansen et al., 2014; Ji et al., 2014; Seamon et al., 2016; Yan et al., 2013; Zhu et al., 2013). Thus, SAMHD1 may function as a monomer or dimer in promoting DNA end resection and tetramer in promoting dNTP metabolism, which is controlled by its binding to ssDNA in response to DNA DSB induction. This may explain, at least in part, why SAMHD1 overexpression, which may facilitate its tetramerization, does not fully rescue the CPT hypersensitivity of SAMHD1 deficiency. Our finding that SAMHD1 promotes DNA end resection provides further support for a common role in nucleic acid metabolism that is shared by SAMHD1 and other AGS susceptibility proteins TREX1, RNaseH2, and ADAR1, suggesting that SAMHD1's role in DNA DSB repair may be important for preventing improper innate immune response and autoimmune disease.

A role for SAMHD1 in maintaining genome integrity and preventing cancer has previously been attributed to its activity in dNTP pool regulation (Clifford et al., 2014; Franzolin et al., 2013; Kohnken et al., 2015; Kretschmer et al., 2015; Rentoft et al., 2016). Our findings now demonstrate that SAMHD1 also has a direct role in genome maintenance by promoting DNA end resection to facilitate DSB repair by HR independent of its canonical role in dNTP metabolism. Given that *SAMHD1* is dysregulated in a number of cancers, SAMHD1's role in DSB repair may help explain, at least in part, how its dysregulation is associated with genomic instability and carcinogenesis. Indeed, our findings show that a naturally occurring gastric cancer-associated *SAMHD1* mutation impairs the interaction of SAMHD1 with CtIP, but not its dNTPase activity, and the mutant SAMHD1 fails to rescue the CtIP recruitment deficit, DNA end resection impairment, and CPT hypersensitivity of SAMHD1 deficiency, suggesting that SAMHD1's interaction with CtIP may be important for the prevention of genomic instability and cancer. As several heterozygous colorectal cancer-associated mutations impair SAMHD1's dNTPase activity, and increased dNTP levels contribute to mutagenesis (Rentoft et al., 2016), collectively, these findings support a role for SAMHD1 in maintaining genome integrity and preventing cancer through dual roles in DNA end resection and dNTP metabolism.

As our data suggest that SAMHD1 plays a critical role in the response of cancer cells to DSB-inducing agents, SAMHD1 may also be a promising therapeutic target for cancer therapies that induce DSBs. Our finding that targeting SAMHD1 for proteasomal degradation with VLPs containing Vpx sensitizes cancer cells to DSB-inducing agents provides rationale for the use of VLPs containing Vpx in augmenting the efficacy of IR, PARP inhibitor, and other DSB-inducing agents as a potential approach for cancer therapy. Another rationale-driven approach for cancer therapy based on our work will be to disrupt the interaction of SAMHD1 and CtIP with small molecule inhibitors to be used as an adjunct to DSB-inducing agents.

EXPERIMENTAL PROCEDURES

Cell Culture, Plasmids, and siRNA

293T, HeLa, HCT-116, MCF7, and U2OS cells were grown in DMEM (GIBCO), supplemented with 7.5% fetal bovine serum (FBS). Stably transfected cells were maintained with 1 μg/mL puromycin (Fisher). SAMHD1-GFP/RFP plasmids were generated by cloning SAMHD1 in pcDNA3.1-GFP/RFP (Addgene, # 70219 or 13032, respectively) using EcoRI/BamHI restriction sites. SAMHD1 WT and truncations were cloned in pKH3 (Addgene, # 12555) using EagI and XbaI to generate SAMHD1-HA. GFP-CtIP, FLAG-CtIP, and GFP-FLAG-MRE11 plasmids were obtained from Dr. Steve Jackson (Sartori et al., 2007; Schmidt et al., 2015). GFP-RPA70 plasmid was obtained from Dr. Marc Wold (Haring et al., 2008). ATRIP-GFP plasmid was obtained from Dr. Akira Matsuura (Itakura et al., 2005). Plasmid transfections were performed using Lipofectamine 2000 (Invitrogen), following manufacture's instruction. Cells

(B) Representative SR images of a single foci showing SAMHD1/CtIP co-localization in cells also labeled for naDNA.
(C) U2OS cells integrated with a DR-GFP HR reporter substrate were transfected with indicated siRNAs and I-SceI, fixed, and analyzed for HR by GFP expression using flow cytometry.
(D) U2OS cells transfected with CtIP, SAMHD1, or NT siRNA were treated with 2 μM CPT for 4 hr, fixed, and processed for immunofluorescence with indicated antibodies. Quantitation of relative percent γH2AX-positive cells with RPA70 foci is shown.
(E) Representative images of GFP-CtIP-expressing U2OS cells transfected with NT or SAMHD1 siRNA, subjected to laser microirradiation, fixed 5 min after damage, and processed for immunofluorescence with anti-γH2AX antibodies.
(F) HCT-116 cells transfected with SAMHD1 or NT siRNA were treated with 10 Gy IR and harvested 1 hr later for biochemical fractionation. Chromatin bound proteins were run on SDS-PAGE and immunoblotted with indicated antibodies. NS indicates non-specific band as loading control.
(G) Representative images of U2OS *SAMHD1* WT and KO cells expressing RFP-SAMHD1 and GFP-CtIP, subjected to laser microirradiation, fixed 5 min after damage, and processed for immunofluorescence with anti-γH2AX antibodies.
(H) U2OS cells were transfected with indicated siRNAs and cDNA, treated with 10 Gy IR, and processed 4 hr later for indirect immunofluorescence with anti-RPA70, HA, and γH2AX antibodies. Quantitation of percent γH2AX-positive cells with RPA70 foci that are SAMHD1-GFP-positive for complemented cells, from three independent replicas of 60 cells counted each is shown.
(I) U2OS cells transfected with indicated siRNAs and plasmids were treated with 200 nM CPT for 72 hr prior to assaying for viability with Alamar Blue. The treated to untreated viability relative to NT siRNA is shown.
(J) Western blot analysis showing expression of SAMHD1-GFP and endogenous SAMHD1 in U2OS cells 72 hr after siRNA transfection and 48 hr after cDNA transfection. The higher levels of SAMHD1 in the SAMHD1-GFP-transfected cells likely represent exogenous SAMHD1 cleaved from SAMHD-GFP.
(A, C, D, H, and I) Mean and SEM from three independent replicas are shown. $^{**}p < 0.01$ and $^{****}p < 0.0001$. See also Figure S6.

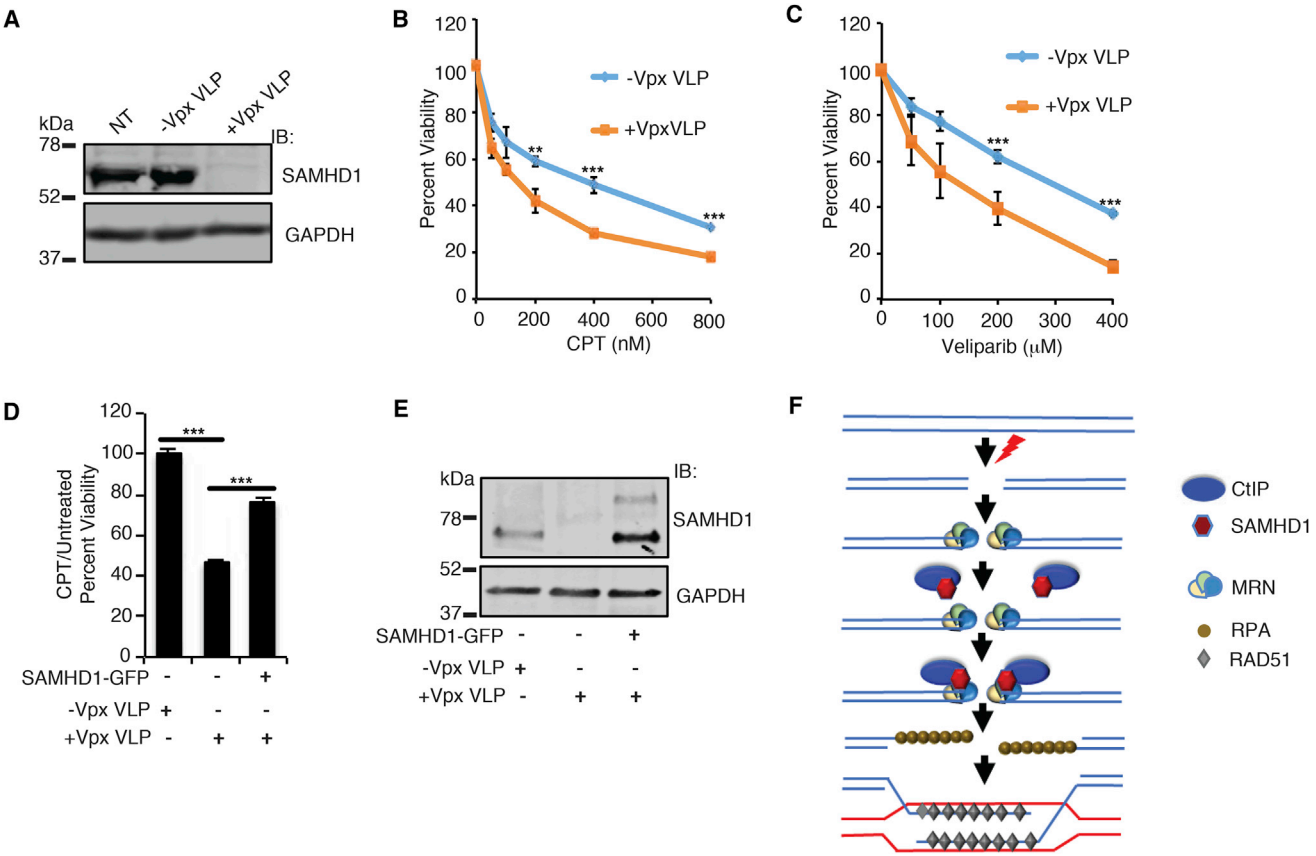

Figure 7. Targeting SAMHD1 with Virus-like Particles Containing Vpx Sensitizes Cancer Cells to DSB-Inducing Agents

(A) Western blot analysis showing SAMHD1 degradation in U2OS cells treated with VLPs containing Vpx or no Vpx for 48 hr.

(B and C) U2OS cells were treated with VLPs containing Vpx or no Vpx for 48 hr, followed by indicated doses of CPT (B) or veliparib (C) for 72 hr and assayed for cell viability using Alamar Blue.

(D) U2OS cells transfected with or without SAMHD-GFP were treated with VLPs containing Vpx or no Vpx for 48 hr followed by 50 nM CPT for 72 hr and assayed for cell viability using Alamar Blue.

(E) Western blot analysis showing expression of SAMHD1-GFP and endogenous SAMHD1 in U2OS cells 72 hr after transfection and 48 hr after treatment with VLPs containing Vpx or no Vpx, at which time cells were treated as in (D). The higher levels of SAMHD1 in the SAMHD1-GFP-transfected and Vpx-treated cells (lower band in third lane) likely results from a combination of endogenous SAMHD1 and exogenous SAMHD1 cleaved from SAMHD-GFP that has not been degraded.

(F) Model showing SAMHD1 function in DNA end resection to facilitate DSB repair by HR. In response to DSB-inducing agents, SAMHD1 interacts with CtIP/MRN in a damage-regulated manner and recruits CtIP to DSBs to promote DNA end resection, facilitating DSB repair by HR.

(B–D) Mean and SEM from three independent replicas are shown. $^{**}p < 0.01$ and $^{***}p < 0.001$.

were transfected with siRNA using Lipofectamine RNAi Max (Invitrogen), following the manufacturer's instructions. siRNAs were purchased from Dharmacon or QIAGEN.

Immunoblot

Cells were harvested in PBS and lysed for 30 min on ice in IP lysis buffer (200 mM NaCl, 0.75% Chaps, and 50 mM Tris pH 8.0) or radioimmunoprecipitation assay (RIPA) buffer (10 mM Tris-Cl [pH 8.0], 1 mM EDTA, 1% Triton X-100, 0.1% sodium deoxycholate, 0.1% SDS, and 140 mM NaCl) (Hall et al., 2014), supplemented with protease inhibitors. Lysates were clarified by centrifugation (13,000 rpm for 10 min at 4°C) and the supernatants were collected. Protein samples were quantified with the Bradford assay and resolved by SDS-PAGE, transferred onto polyvinylidene fluoride (PVDF), and probed using the indicated primary antibodies. The membrane was stained with Alexa Fluor 680 or 800 anti-mouse/rabbit secondary antibody (Life Technologies) and visualized with the LI-COR Odyssey system. The following antibodies were used for staining: GAPDH (Santa Cruz, sc-47724); FLAG (Santa Cruz, sc-51590); GFP (Abcam, Ab6556); HA (Sigma, H9658), RPA70 (Cell Signal, 2267), RPA32 (Santa Cruz, sc-14692), SAMHD1 (OriGene, TA502024), CtIP (14-1, a generous gift from Richard Baer) (Yu and Baer, 2000), BRCA2, RAD51 (Calbiochem, PC130), γH2AX (Cell Signal, 2577 or Millipore, 05-636), 53BP1 (Bethyl Labs, A300-273A), BrdU (BD Biosciences, 347580), and MRE11 (Abcam, ab30725).

Cell Viability Assay

Cell viability assays were performed as previously described (Colbert et al., 2014; Smith et al., 2014; Yu et al., 2010; Zhang et al., 2013). Briefly, cells were plated at a density of 5×10^5 cells/well in 6-well plates and siRNA transfected at 25 nM. 24 hr post knockdown, media were replaced with or without overexpression solution containing media supplemented with plasmid DNA, Lipofectamine 2000, and Opti-MEM solution. Cells were treated with VLP containing Vpx or no Vpx, as described previously (Berger et al., 2011; Kim et al., 2012), with minor modification. 24 hr after initial transfection or transduction with Vpx VLPs, cells were trypsinized, counted, and replated in triplicate to a

density of 2 × 10^3 cells/well in 96-well plates. 24 hr after plating, cells were treated with media containing the drug for 72 hr. Cell viability was then assessed via Alamar Blue (resazurin) reagent, incubated at 1:10 dilution for 6 hr, and assayed for fluorescence according to the manufacturer's protocol. Viability fractions were normalized to vehicle-treated controls exposed to identical transfection conditions.

Statistical Analysis

Unless otherwise stated, experiments were performed at least three times and analyzed using unpaired two-tailed Student's t test and data expressed as mean ± SEM, $p < 0.05$ was considered statistically significant.

IP, Immunofluorescence, Clonogenic Assay, DSB Repair Reporter Assay, Laser Microirradiation Assay, DNA End Resection, Comet Assay, dNTP Pool Quantitation, KO Cell Generation, Chromatin Fractionation Assay, SR Imaging.

Details of these methodologies can be found in Supplemental Experimental Procedures.

ACCESSION NUMBERS

The accession number for SAMHD1 crystal structure used to generate a Figure S5D is RCSB PDB: 4BZB.

SUPPLEMENTAL INFORMATION

Supplemental Information includes Supplemental Experimental Procedures and seven figures and can be found with this article online at http://dx.doi.org/10.1016/j.celrep.2017.08.008.

AUTHOR CONTRIBUTIONS

Conceptualization, W.D., X.D., W.S.D., Y.W., R.S.B., P.W.D., B.K., and D.S.Y.; Investigation, W.D., A.E.K., W.S.D., P.E.H., V.R.D., E.C.C., A.J.B., E.W., G.N.N., M.Z.M., M.B.D., E.V.M., D.R.W., A.J.S., H.Z., R.A., C.D., A.E.W., C.S., and R.K.S.; Writing - Original Draft, W.D. and D.S.Y.; Writing - Review and Editing, W.D., A.E.K., W.S.D., P.E.H., E.C.C., A.J.B., E.W., G.N.N., M.Z.M., M.B.D., E.V.M., D.R.W., R.A., H.Z., A.J.S., C.D., A.E.W., C.S., R.K.S., X.D., W.S.D., Y.W., R.S.B., P.C., E.R., P.W.D., B.K., and D.S.Y.; Supervision, W.D., X.D., W.S.D., Y.W., R.S.B., P.C., E.R., P.W.D., B.K., and D.S.Y.; and Funding Acquisition, W.D., X.D., and D.S.Y.

ACKNOWLEDGMENTS

We thank Dr. Tatsuya Maehigashi and Russell Goetze for SAMHD1 and Vpx purification; Dr. Steve Jackson for GFP-CtIP, FLAG-CtIP, and GFP-FLAG-MRE11; Dr. Marc Wold for GFP-RPA70; Dr. Akira Matsuura for ATRIP-GFP plasmids; Dr. Maria Jasin for DR-GFP HR reporter plasmid; Dr. Vera Gorbunova for the pEGFP-Pem1-Ad2 NHEJ reporter plasmid; and Dr. Richard Baer for CtIP antibody. This work was supported by NIH/NCI R01CA178999 and R01CA178999S1 and DOD/PRCRP CA160771 to D.S.Y., NIH/NIGMS F32 GM121071-01 to W.D., NIH/NCI 2R01CA136534 to X.D., and NIH/NIAID R01AI049781 and NIH/NIGMS R01GM104198 to B.K.

Received: April 7, 2017
Revised: July 5, 2017
Accepted: July 28, 2017
Published: August 22, 2017

REFERENCES

Anand, R., Ranjha, L., Cannavo, E., and Cejka, P. (2016). Phosphorylated CtIP functions as a Co-factor of the MRE11-RAD50-NBS1 endonuclease in DNA end resection. Mol. Cell *64*, 940–950.

Antonucci, J.M., St Gelais, C., de Silva, S., Yount, J.S., Tang, C., Ji, X., Shepard, C., Xiong, Y., Kim, B., and Wu, L. (2016). SAMHD1-mediated HIV-1 restriction in cells does not involve ribonuclease activity. Nat. Med. *22*, 1072–1074.

Aravind, L., and Koonin, E.V. (1998). The HD domain defines a new superfamily of metal-dependent phosphohydrolases. Trends Biochem. Sci. *23*, 469–472.

Baldauf, H.M., Pan, X., Erikson, E., Schmidt, S., Daddacha, W., Burggraf, M., Schenkova, K., Ambiel, I., Wabnitz, G., Gramberg, T., et al. (2012). SAMHD1 restricts HIV-1 infection in resting CD4(+) T cells. Nat. Med. *18*, 1682–1687.

Beloglazova, N., Flick, R., Tchigvintsev, A., Brown, G., Popovic, A., Nocek, B., and Yakunin, A.F. (2013). Nuclease activity of the human SAMHD1 protein implicated in the Aicardi-Goutieres syndrome and HIV-1 restriction. J. Biol. Chem. *288*, 8101–8110.

Berger, G., Durand, S., Goujon, C., Nguyen, X.N., Cordeil, S., Darlix, J.L., and Cimarelli, A. (2011). A simple, versatile and efficient method to genetically modify human monocyte-derived dendritic cells with HIV-1-derived lentiviral vectors. Nat. Protoc. *6*, 806–816.

Brandariz-Nuñez, A., Valle-Casuso, J.C., White, T.E., Nguyen, L., Bhattacharya, A., Wang, Z., Demeler, B., Amie, S., Knowlton, C., Kim, B., et al. (2013). Contribution of oligomerization to the anti-HIV-1 properties of SAMHD1. Retrovirology *10*, 131.

Cannavo, E., and Cejka, P. (2014). Sae2 promotes dsDNA endonuclease activity within Mre11-Rad50-Xrs2 to resect DNA breaks. Nature *514*, 122–125.

Cejka, P., Plank, J.L., Bachrati, C.Z., Hickson, I.D., and Kowalczykowski, S.C. (2010). Rmi1 stimulates decatenation of double Holliday junctions during dissolution by Sgs1-Top3. Nat. Struct. Mol. Biol. *17*, 1377–1382.

Cerami, E., Gao, J., Dogrusoz, U., Gross, B.E., Sumer, S.O., Aksoy, B.A., Jacobsen, A., Byrne, C.J., Heuer, M.L., Larsson, E., et al. (2012). The cBio cancer genomics portal: an open platform for exploring multidimensional cancer genomics data. Cancer Discov. *2*, 401–404.

Clifford, R., Louis, T., Robbe, P., Ackroyd, S., Burns, A., Timbs, A.T., Wright Colopy, G., Dreau, H., Sigaux, F., Judde, J.G., et al. (2014). SAMHD1 is mutated recurrently in chronic lymphocytic leukemia and is involved in response to DNA damage. Blood *123*, 1021–1031.

Colbert, L.E., Petrova, A.V., Fisher, S.B., Pantazides, B.G., Madden, M.Z., Hardy, C.W., Warren, M.D., Pan, Y., Nagaraju, G.P., Liu, E.A., et al. (2014). CHD7 expression predicts survival outcomes in patients with resected pancreatic cancer. Cancer Res. *74*, 2677–2687.

Franzolin, E., Pontarin, G., Rampazzo, C., Miazzi, C., Ferraro, P., Palumbo, E., Reichard, P., and Bianchi, V. (2013). The deoxynucleotide triphosphohydrolase SAMHD1 is a major regulator of DNA precursor pools in mammalian cells. Proc. Natl. Acad. Sci. USA *110*, 14272–14277.

Garcia, V., Phelps, S.E., Gray, S., and Neale, M.J. (2011). Bidirectional resection of DNA double-strand breaks by Mre11 and Exo1. Nature *479*, 241–244.

Goldstone, D.C., Ennis-Adeniran, V., Hedden, J.J., Groom, H.C., Rice, G.I., Christodoulou, E., Walker, P.A., Kelly, G., Haire, L.F., Yap, M.W., et al. (2011). HIV-1 restriction factor SAMHD1 is a deoxynucleoside triphosphate triphosphohydrolase. Nature *480*, 379–382.

Goncalves, A., Karayel, E., Rice, G.I., Bennett, K.L., Crow, Y.J., Superti-Furga, G., and Bürckstümmer, T. (2012). SAMHD1 is a nucleic-acid binding protein that is mislocalized due to aicardi-goutières syndrome-associated mutations. Hum. Mutat. *33*, 1116–1122.

Gravel, S., Chapman, J.R., Magill, C., and Jackson, S.P. (2008). DNA helicases Sgs1 and BLM promote DNA double-strand break resection. Genes Dev. *22*, 2767–2772.

Hall, W.A., Petrova, A.V., Colbert, L.E., Hardy, C.W., Fisher, S.B., Saka, B., Shelton, J.W., Warren, M.D., Pantazides, B.G., Gandhi, K., et al. (2014). Low CHD5 expression activates the DNA damage response and predicts poor outcome in patients undergoing adjuvant therapy for resected pancreatic cancer. Oncogene *33*, 5450–5456.

Hansen, E.C., Seamon, K.J., Cravens, S.L., and Stivers, J.T. (2014). GTP activator and dNTP substrates of HIV-1 restriction factor SAMHD1 generate a long-lived activated state. Proc. Natl. Acad. Sci. USA *111*, E1843–E1851.

Haring, S.J., Mason, A.C., Binz, S.K., and Wold, M.S. (2008). Cellular functions of human RPA1. Multiple roles of domains in replication, repair, and checkpoints. J. Biol. Chem. *283*, 19095–19111.

Helleday, T., Bryant, H.E., and Schultz, N. (2005). Poly(ADP-ribose) polymerase (PARP-1) in homologous recombination and as a target for cancer therapy. Cell Cycle *4*, 1176–1178.

Herold, N., Rudd, S.G., Ljungblad, L., Sanjiv, K., Myrberg, I.H., Paulin, C.B., Heshmati, Y., Hagenkort, A., Kutzner, J., Page, B.D., et al. (2017). Targeting SAMHD1 with the Vpx protein to improve cytarabine therapy for hematological malignancies. Nat. Med. *23*, 256–263.

Hollenbaugh, J.A., Shelton, J., Tao, S., Amiralaei, S., Liu, P., Lu, X., Goetze, R.W., Zhou, L., Nettles, J.H., Schinazi, R.F., and Kim, B. (2017). Substrates and inhibitors of SAMHD1. PLoS ONE *12*, e0169052.

Hrecka, K., Hao, C., Gierszewska, M., Swanson, S.K., Kesik-Brodacka, M., Srivastava, S., Florens, L., Washburn, M.P., and Skowronski, J. (2011). Vpx relieves inhibition of HIV-1 infection of macrophages mediated by the SAMHD1 protein. Nature *474*, 658–661.

Itakura, E., Sawada, I., and Matsuura, A. (2005). Dimerization of the ATRIP protein through the coiled-coil motif and its implication to the maintenance of stalled replication forks. Mol. Biol. Cell *16*, 5551–5562.

Jackson, S.P., and Bartek, J. (2009). The DNA-damage response in human biology and disease. Nature *461*, 1071–1078.

Ji, X., Wu, Y., Yan, J., Mehrens, J., Yang, H., DeLucia, M., Hao, C., Gronenborn, A.M., Skowronski, J., Ahn, J., and Xiong, Y. (2013). Mechanism of allosteric activation of SAMHD1 by dGTP. Nat. Struct. Mol. Biol. *20*, 1304–1309.

Ji, X., Tang, C., Zhao, Q., Wang, W., and Xiong, Y. (2014). Structural basis of cellular dNTP regulation by SAMHD1. Proc. Natl. Acad. Sci. USA *111*, E4305–E4314.

Kim, B., Nguyen, L.A., Daddacha, W., and Hollenbaugh, J.A. (2012). Tight interplay among SAMHD1 protein level, cellular dNTP levels, and HIV-1 proviral DNA synthesis kinetics in human primary monocyte-derived macrophages. J. Biol. Chem. *287*, 21570–21574.

Kohnken, R., Kodigepalli, K.M., and Wu, L. (2015). Regulation of deoxynucleotide metabolism in cancer: novel mechanisms and therapeutic implications. Mol. Cancer *14*, 176.

Kretschmer, S., Wolf, C., König, N., Staroske, W., Guck, J., Häusler, M., Luksch, H., Nguyen, L.A., Kim, B., Alexopoulou, D., et al. (2015). SAMHD1 prevents autoimmunity by maintaining genome stability. Ann. Rheum. Dis. *74*, e17.

Laguette, N., Sobhian, B., Casartelli, N., Ringeard, M., Chable-Bessia, C., Ségéral, E., Yatim, A., Emiliani, S., Schwartz, O., and Benkirane, M. (2011). SAMHD1 is the dendritic- and myeloid-cell-specific HIV-1 restriction factor counteracted by Vpx. Nature *474*, 654–657.

Lahouassa, H., Daddacha, W., Hofmann, H., Ayinde, D., Logue, E.C., Dragin, L., Bloch, N., Maudet, C., Bertrand, M., Gramberg, T., et al. (2012). SAMHD1 restricts the replication of human immunodeficiency virus type 1 by depleting the intracellular pool of deoxynucleoside triphosphates. Nat. Immunol. *13*, 223–228.

Limbo, O., Chahwan, C., Yamada, Y., de Bruin, R.A., Wittenberg, C., and Russell, P. (2007). Ctp1 is a cell-cycle-regulated protein that functions with Mre11 complex to control double-strand break repair by homologous recombination. Mol. Cell *28*, 134–146.

Makharashvili, N., Tubbs, A.T., Yang, S.H., Wang, H., Barton, O., Zhou, Y., Deshpande, R.A., Lee, J.H., Lobrich, M., Sleckman, B.P., et al. (2014). Catalytic and noncatalytic roles of the CtIP endonuclease in double-strand break end resection. Mol. Cell *54*, 1022–1033.

Mimitou, E.P., and Symington, L.S. (2008). Sae2, Exo1 and Sgs1 collaborate in DNA double-strand break processing. Nature *455*, 770–774.

Nicolette, M.L., Lee, K., Guo, Z., Rani, M., Chow, J.M., Lee, S.E., and Paull, T.T. (2010). Mre11-Rad50-Xrs2 and Sae2 promote 5′ strand resection of DNA double-strand breaks. Nat. Struct. Mol. Biol. *17*, 1478–1485.

Nimonkar, A.V., Genschel, J., Kinoshita, E., Polaczek, P., Campbell, J.L., Wyman, C., Modrich, P., and Kowalczykowski, S.C. (2011). BLM-DNA2-RPA-MRN and EXO1-BLM-RPA-MRN constitute two DNA end resection machineries for human DNA break repair. Genes Dev. *25*, 350–362.

Niu, H., Chung, W.H., Zhu, Z., Kwon, Y., Zhao, W., Chi, P., Prakash, R., Seong, C., Liu, D., Lu, L., et al. (2010). Mechanism of the ATP-dependent DNA end-resection machinery from Saccharomyces cerevisiae. Nature *467*, 108–111.

Paull, T.T., and Gellert, M. (1998). The 3′ to 5′ exonuclease activity of Mre 11 facilitates repair of DNA double-strand breaks. Mol. Cell *1*, 969–979.

Pierce, A.J., Johnson, R.D., Thompson, L.H., and Jasin, M. (1999). XRCC3 promotes homology-directed repair of DNA damage in mammalian cells. Genes Dev. *13*, 2633–2638.

Powell, R.D., Holland, P.J., Hollis, T., and Perrino, F.W. (2011). Aicardi-Goutieres syndrome gene and HIV-1 restriction factor SAMHD1 is a dGTP-regulated deoxynucleotide triphosphohydrolase. J. Biol. Chem. *286*, 43596–43600.

Prakash, R., Zhang, Y., Feng, W., and Jasin, M. (2015). Homologous recombination and human health: the roles of BRCA1, BRCA2, and associated proteins. Cold Spring Harb. Perspect. Biol. *7*, a016600.

Rentoft, M., Lindell, K., Tran, P., Chabes, A.L., Buckland, R.J., Watt, D.L., Marjavaara, L., Nilsson, A.K., Melin, B., Trygg, J., et al. (2016). Heterozygous colon cancer-associated mutations of SAMHD1 have functional significance. Proc. Natl. Acad. Sci. USA *113*, 4723–4728.

Rice, G.I., Bond, J., Asipu, A., Brunette, R.L., Manfield, I.W., Carr, I.M., Fuller, J.C., Jackson, R.M., Lamb, T., Briggs, T.A., et al. (2009). Mutations involved in Aicardi-Goutières syndrome implicate SAMHD1 as regulator of the innate immune response. Nat. Genet. *41*, 829–832.

Ryoo, J., Choi, J., Oh, C., Kim, S., Seo, M., Kim, S.Y., Seo, D., Kim, J., White, T.E., Brandariz-Nuñez, A., et al. (2014). The ribonuclease activity of SAMHD1 is required for HIV-1 restriction. Nat. Med. *20*, 936–941.

Sartori, A.A., Lukas, C., Coates, J., Mistrik, M., Fu, S., Bartek, J., Baer, R., Lukas, J., and Jackson, S.P. (2007). Human CtIP promotes DNA end resection. Nature *450*, 509–514.

Schmidt, C.K., Galanty, Y., Sczaniecka-Clift, M., Coates, J., Jhujh, S., Demir, M., Cornwell, M., Beli, P., and Jackson, S.P. (2015). Systematic E2 screening reveals a UBE2D-RNF138-CtIP axis promoting DNA repair. Nat. Cell Biol. *17*, 1458–1470.

Schneider, C., Oellerich, T., Baldauf, H.M., Schwarz, S.M., Thomas, D., Flick, R., Bohnenberger, H., Kaderali, L., Stegmann, L., Cremer, A., et al. (2017). SAMHD1 is a biomarker for cytarabine response and a therapeutic target in acute myeloid leukemia. Nat. Med. *23*, 250–255.

Schultz, J., Ponting, C.P., Hofmann, K., and Bork, P. (1997). SAM as a protein interaction domain involved in developmental regulation. Protein Sci. *6*, 249–253.

Seamon, K.J., Sun, Z., Shlyakhtenko, L.S., Lyubchenko, Y.L., and Stivers, J.T. (2015). SAMHD1 is a single-stranded nucleic acid binding protein with no active site-associated nuclease activity. Nucleic Acids Res. *43*, 6486–6499.

Seamon, K.J., Bumpus, N.N., and Stivers, J.T. (2016). Single-stranded nucleic acids bind to the tetramer interface of SAMHD1 and prevent formation of the catalytic homotetramer. Biochemistry *55*, 6087–6099.

Seluanov, A., Mittelman, D., Pereira-Smith, O.M., Wilson, J.H., and Gorbunova, V. (2004). DNA end joining becomes less efficient and more error-prone during cellular senescence. Proc. Natl. Acad. Sci. USA *101*, 7624–7629.

Smith, S.C., Petrova, A.V., Madden, M.Z., Wang, H., Pan, Y., Warren, M.D., Hardy, C.W., Liang, D., Liu, E.A., Robinson, M.H., et al. (2014). A gemcitabine sensitivity screen identifies a role for NEK9 in the replication stress response. Nucleic Acids Res. *42*, 11517–11527.

Stracker, T.H., and Petrini, J.H. (2011). The MRE11 complex: starting from the ends. Nat. Rev. Mol. Cell Biol. *12*, 90–103.

Symington, L.S., and Gautier, J. (2011). Double-strand break end resection and repair pathway choice. Annu. Rev. Genet. *45*, 247–271.

Tüngler, V., Staroske, W., Kind, B., Dobrick, M., Kretschmer, S., Schmidt, F., Krug, C., Lorenz, M., Chara, O., Schwille, P., and Lee-Kirsch, M.A. (2013). Single-stranded nucleic acids promote SAMHD1 complex formation. J. Mol. Med. (Berl.) *91*, 759–770.

Wang, H., Shao, Z., Shi, L.Z., Hwang, P.Y., Truong, L.N., Berns, M.W., Chen, D.J., and Wu, X. (2012). CtIP protein dimerization is critical for its recruitment to chromosomal DNA double-stranded breaks. J. Biol. Chem. *287*, 21471–21480.

Wang, H., Li, Y., Truong, L.N., Shi, L.Z., Hwang, P.Y., He, J., Do, J., Cho, M.J., Li, H., Negrete, A., et al. (2014). CtIP maintains stability at common fragile sites and inverted repeats by end resection-independent endonuclease activity. Mol. Cell *54*, 1012–1021.

Welbourn, S., and Strebel, K. (2016). Low dNTP levels are necessary but may not be sufficient for lentiviral restriction by SAMHD1. Virology *488*, 271–277.

Whelan, D.R., Yin, Y., Bermudez-Hernandez, K., Keegan, S., Fenyö, D., and Rothenberg, E. (2016). Single molecule localization microscopy of DNA damage response pathways in cancer. Microsc. Microanal. *22* (*Suppl 3*), 1016–1017.

Yan, J., Kaur, S., DeLucia, M., Hao, C., Mehrens, J., Wang, C., Golczak, M., Palczewski, K., Gronenborn, A.M., Ahn, J., and Skowronski, J. (2013). Tetramerization of SAMHD1 is required for biological activity and inhibition of HIV infection. J. Biol. Chem. *288*, 10406–10417.

You, Z., Shi, L.Z., Zhu, Q., Wu, P., Zhang, Y.W., Basilio, A., Tonnu, N., Verma, I.M., Berns, M.W., and Hunter, T. (2009). CtIP links DNA double-strand break sensing to resection. Mol. Cell *36*, 954–969.

Yu, X., and Baer, R. (2000). Nuclear localization and cell cycle-specific expression of CtIP, a protein that associates with the BRCA1 tumor suppressor. J. Biol. Chem. *275*, 18541–18549.

Yu, X., Fu, S., Lai, M., Baer, R., and Chen, J. (2006). BRCA1 ubiquitinates its phosphorylation-dependent binding partner CtIP. Genes Dev. *20*, 1721–1726.

Yu, D.S., Zhao, R., Hsu, E.L., Cayer, J., Ye, F., Guo, Y., Shyr, Y., and Cortez, D. (2010). Cyclin-dependent kinase 9-cyclin K functions in the replication stress response. EMBO Rep. *11*, 876–882.

Yuan, J., and Chen, J. (2009). N terminus of CtIP is critical for homologous recombination-mediated double-strand break repair. J. Biol. Chem. *284*, 31746–31752.

Zhang, H., Park, S.H., Pantazides, B.G., Karpiuk, O., Warren, M.D., Hardy, C.W., Duong, D.M., Park, S.J., Kim, H.S., Vassilopoulos, A., et al. (2013). SIRT2 directs the replication stress response through CDK9 deacetylation. Proc. Natl. Acad. Sci. USA *110*, 13546–13551.

Zhang, H., Head, P.E., Daddacha, W., Park, S.H., Li, X., Pan, Y., Madden, M.Z., Duong, D.M., Xie, M., Yu, B., et al. (2016). ATRIP deacetylation by SIRT2 drives ATR checkpoint activation by promoting binding to RPA-ssDNA. Cell Rep. *14*, 1435–1447.

Zhu, Z., Chung, W.H., Shim, E.Y., Lee, S.E., and Ira, G. (2008). Sgs1 helicase and two nucleases Dna2 and Exo1 resect DNA double-strand break ends. Cell *134*, 981–994.

Zhu, C., Gao, W., Zhao, K., Qin, X., Zhang, Y., Peng, X., Zhang, L., Dong, Y., Zhang, W., Li, P., et al. (2013). Structural insight into dGTP-dependent activation of tetrameric SAMHD1 deoxynucleoside triphosphate triphosphohydrolase. Nat. Commun. *4*, 2722.

Zou, L., and Elledge, S.J. (2003). Sensing DNA damage through ATRIP recognition of RPA-ssDNA complexes. Science *300*, 1542–1548.

Cell Reports, Volume *20*

Supplemental Information

SAMHD1 Promotes DNA End Resection to Facilitate DNA Repair by Homologous Recombination

Waaqo Daddacha, Allyson E. Koyen, Amanda J. Bastien, PamelaSara E. Head, Vishal R. Dhere, Geraldine N. Nabeta, Erin C. Connolly, Erica Werner, Matthew Z. Madden, Michele B. Daly, Elizabeth V. Minten, Donna R. Whelan, Ashley J. Schlafstein, Hui Zhang, Roopesh Anand, Christine Doronio, Allison E. Withers, Caitlin Shepard, Ranjini K. Sundaram, Xingming Deng, William S. Dynan, Ya Wang, Ranjit S. Bindra, Petr Cejka, Eli Rothenberg, Paul W. Doetsch, Baek Kim, and David S. Yu

Supplemental Information

SUPPLEMENTAL DATA ITEMS

Figure S1 is related to Figure 1
Figure S2 is related to Figure 2
Figure S3 is related to Figure 3
Figure S4 is related to Figure 4
Figure S5 is related to Figure 5
Figure S6 is related to Figure 6
Figure S7 is related to Figures 1-7

SUPPLEMENTAL EXPERIMENTAL PROCEDURES

SUPPLEMENTAL REFERENCES

SUPPLEMENTAL DATA ITEMS

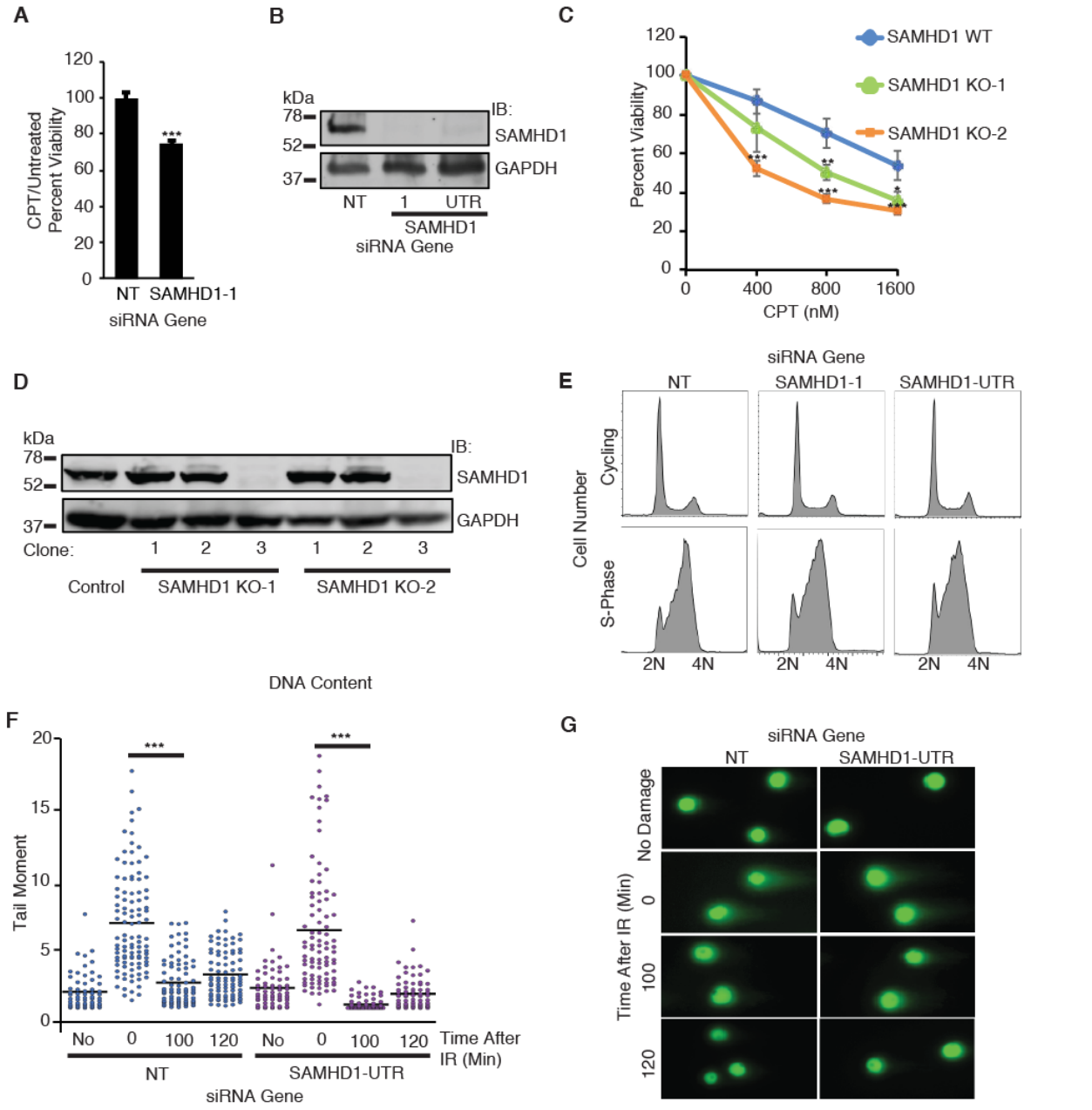

Figure S1 is Related to Figure 1. SAMHD1 Functions in DNA DSB Repair. (A) BEAS-2B cells transfected with SAMHD1 or NT siRNA were treated with 800 nM CPT for 72 h prior to assaying for cell viability with AlamarBlue. Treated to untreated viability relative to NT siRNA was determined. **(B)** Western blot analysis showing SAMHD1 knockdown in BEAS-2B cells 72 h after transfection. **(C)** HCT-116 WT and SAMHD1 KO (KO1 and KO2) cells were treated with indicated doses of CPT for 72 h and assayed for cell viability using AlamarBlue. **(D)** Western blot analysis of lysate from HCT-116 WT and SAMHD1 KO cells generated by CRISPR/Cas9 with two unique guide RNAs (gRNA1 and gRNA2). **(E)** U2OS cells transfected with indicated siRNAs were synchronized by 16 h mimosine arrest followed by a 7 h release. DNA content of synchronized and unsynchronized cells was analyzed by flow cytometry. **(F-G)** Unsynchronized U2OS cells transfected with indicated siRNAs were treated with or without 10 Gy IR and allowed to recover for the indicated times. DNA damage was analyzed by neutral comet assay. **(F)** Dot plot with median of comet tail moment is shown. *** $p < 0.001$. **(G)** Representative images of comet tails are shown.

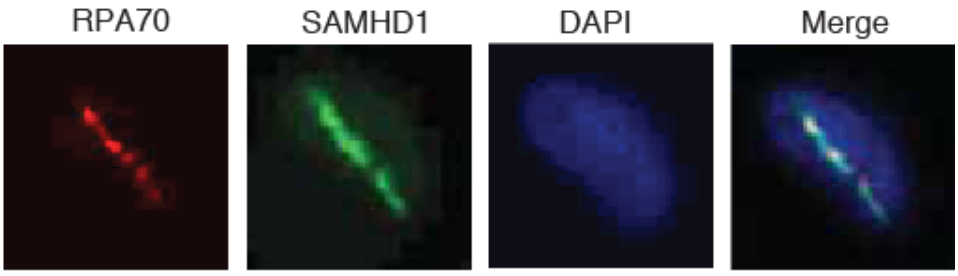

Figure S2 is Related to Figure 2. SAMHD1 Localizes to DSBs in Response to DNA Damage. U2OS cells were microirradiated with a Photonics 365 nM laser, fixed after 1 min, and processed for indirect immunofluorescence with anti-RPA70 and γH2AX antibodies.

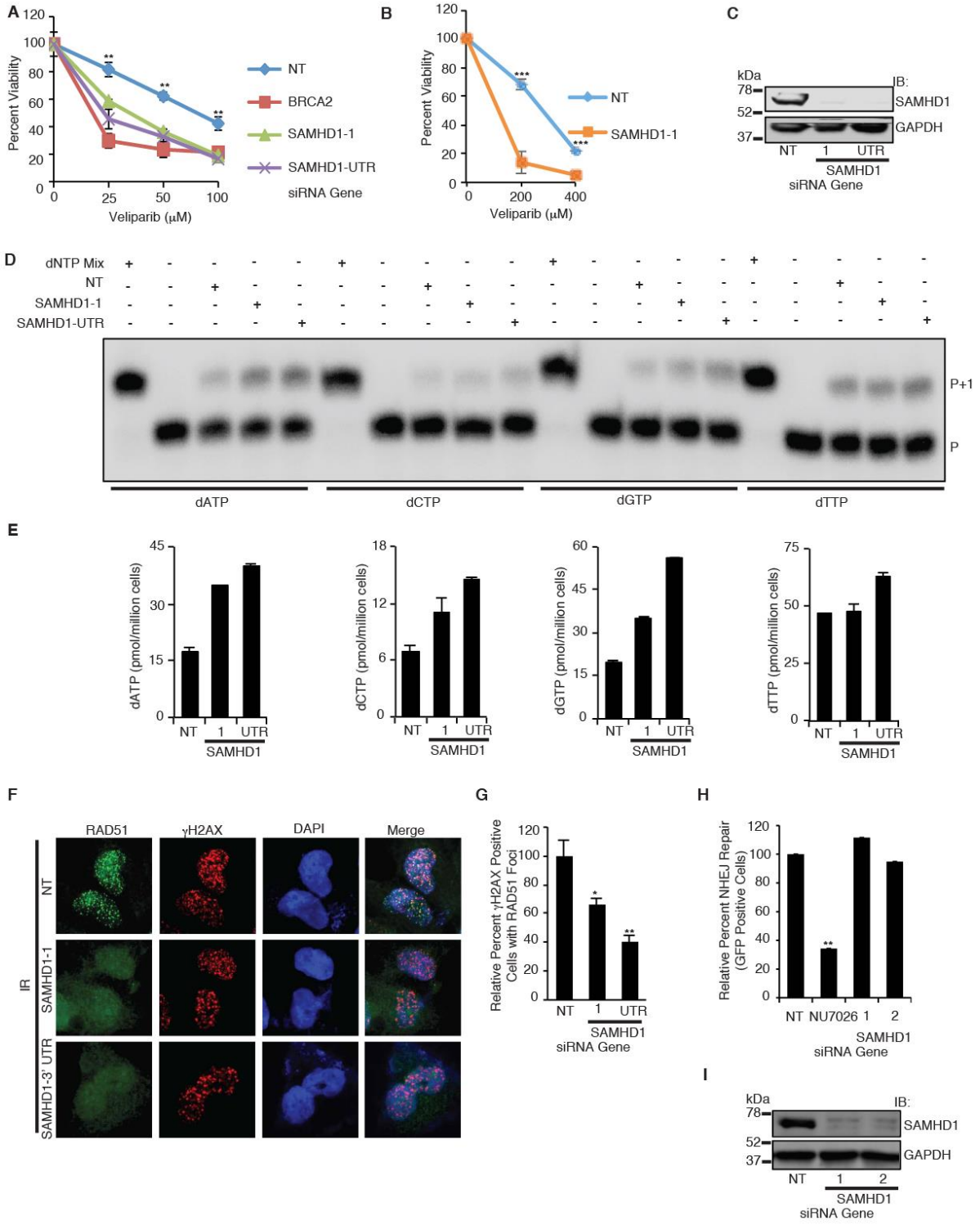

Figure S3 is Related to Figure 3. SAMHD1 Functions in DSB Repair by Facilitating HR. (A) MCF7 cells transfected with indicated siRNAs were treated with indicated doses of Veliparib for 72 h and assayed for cell viability using AlamarBlue. **(B)** Primary small airway epithelial cells transfected with SAMHD1 or NT siRNA were treated with indicated doses of Veliparib for 72 h and assayed for cell viability using AlamarBlue. **(C)** Western blot analysis showing SAMHD1 knockdown in primary small airway epithelial cells 72 h after transfection. **(D)** dNTP samples extracted from U2OS cells depleted of SAMHD1 were used to perform a RT based primer extension assay

to determine dATP, dCTP, dGTP and dTTP concentrations. Shown is representative gel image. **(E)** Mean and SEM of dNTP concentration from three replicas is shown. **(F-G)** BEAS-2B cells transfected with SAMHD1 or NT siRNA were treated with 10 Gy IR, fixed 4 h later, and processed for indirect immunofluorescence with anti-RAD51 and γH2AX antibodies. **(F)** Representative images showing impairment in IR-induced RAD51 but not γH2AX foci by SAMHD1 depletion are shown. **(G)** Quantitation of relative percent γH2AX positive cells with RAD51 foci from 3 independent replicas of at least 200 cells counted each is shown. **(H)** U2OS cells were transfected with indicated siRNAs and the pEGFP-Pem1-Ad2 NHEJ reporter substrate following I-SceI digestion, fixed, and analyzed for NHEJ by GFP expression using flow cytometry. Relative percent NHEJ repair (GFP-positive cells) is shown. **(I)** Western blot analysis showing SAMHD1 knockdown in U2OS cells 72 h after transfection. For **(A**), **(B)**, **(G)**, and **(H)**, mean and SEM from three independent replicas is shown. * $p < 0.05$, ** $p < 0.01$, *** $p < 0.001$.

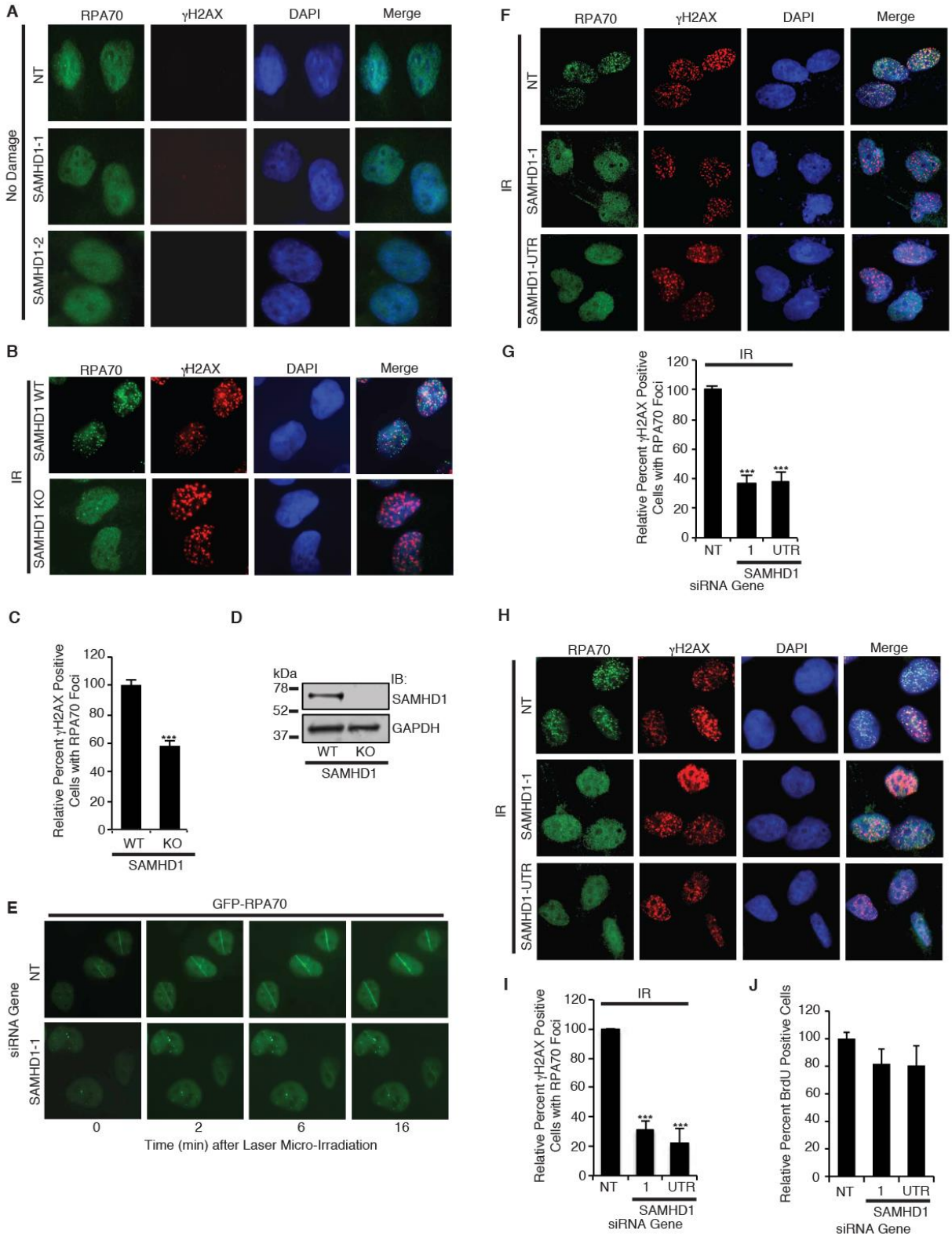

Figure S4 is Related to Figure 4. SAMHD1 Facilitates HR by Promoting DNA End Resection. (A) Nondamaged U2OS cells transfected with SAMHD1 or NT siRNA were fixed and processed for indirect immunofluorescence with anti-RPA70 and γH2AX antibodies. Representative images are shown. **(B-C)** U2OS

SAMHD1 WT and KO cells were treated with 10 Gy IR, fixed 4 h later, and processed for indirect immunofluorescence with anti-RPA70 and γH2AX antibodies. **(B)** Representative images showing impairment in IR-induced RPA70 but not γH2AX foci with SAMHD1 knockout is shown. **(C)** Quantitation of relative percent γH2AX positive cells with RPA70 foci from 3 independent replicas of 200 cells counted each is shown. **(D)** Western blot analysis of lysate from U2OS WT and SAMHD1 KO cells generated by CRISPR/Cas9. **(E)** Representative live-cell images of GFP-RPA70 expressing U2OS cells transfected with NT or SAMHD1 siRNA, subjected to laser micro-irradiation, and monitored in real-time by direct immunofluorescence. **(F-G)** BEAS-2B cells transfected with SAMHD1 or NT siRNA were treated with 10 Gy IR, fixed 4 h later, and processed for indirect immunofluorescence with anti-RPA70 and γH2AX antibodies. **(F)** Representative images showing impairment in IR-induced RPA70 but not γH2AX foci with SAMHD1 depletion are presented. **(G)** Quantitation of relative percent γH2AX positive cells with RPA70 foci from 3 independent replicas of 200 cells counted each is shown. **(H-I)** Primary small airway epithelial cells transfected with SAMHD1 or NT siRNA were treated with 10 Gy IR, fixed 4 h later, and processed for indirect immunofluorescence with anti-RPA70 and γH2AX antibodies. **(H)** Representative images showing impairment in IR-induced RPA70 but not γH2AX foci with SAMHD1 depletion is shown. **(I)** Quantitation of relative percent γH2AX positive cells with RPA70 foci from 3 independent replicas of 200 cells counted each is shown. **(J)** Quantitation of BrdU incorporation under denaturing conditions for SAMHD1 depleted U2OS cells treated with 30 µM BrdU for 36 h followed by 3µM CPT treatment for 4 h. Cells were fixed, denatured with HCl, and processed for indirect immunofluorescence using anti-BrdU antibodies. Mean and SEM from three replicas is shown. A mild but not statistically significant decrease in BrdU uptake between SAMHD1 and NT depletion was observed. For **(C**), **(G)**, **(I)**, and **(J)**, mean and SEM from three independent replicas is shown. *** $p < 0.001$.

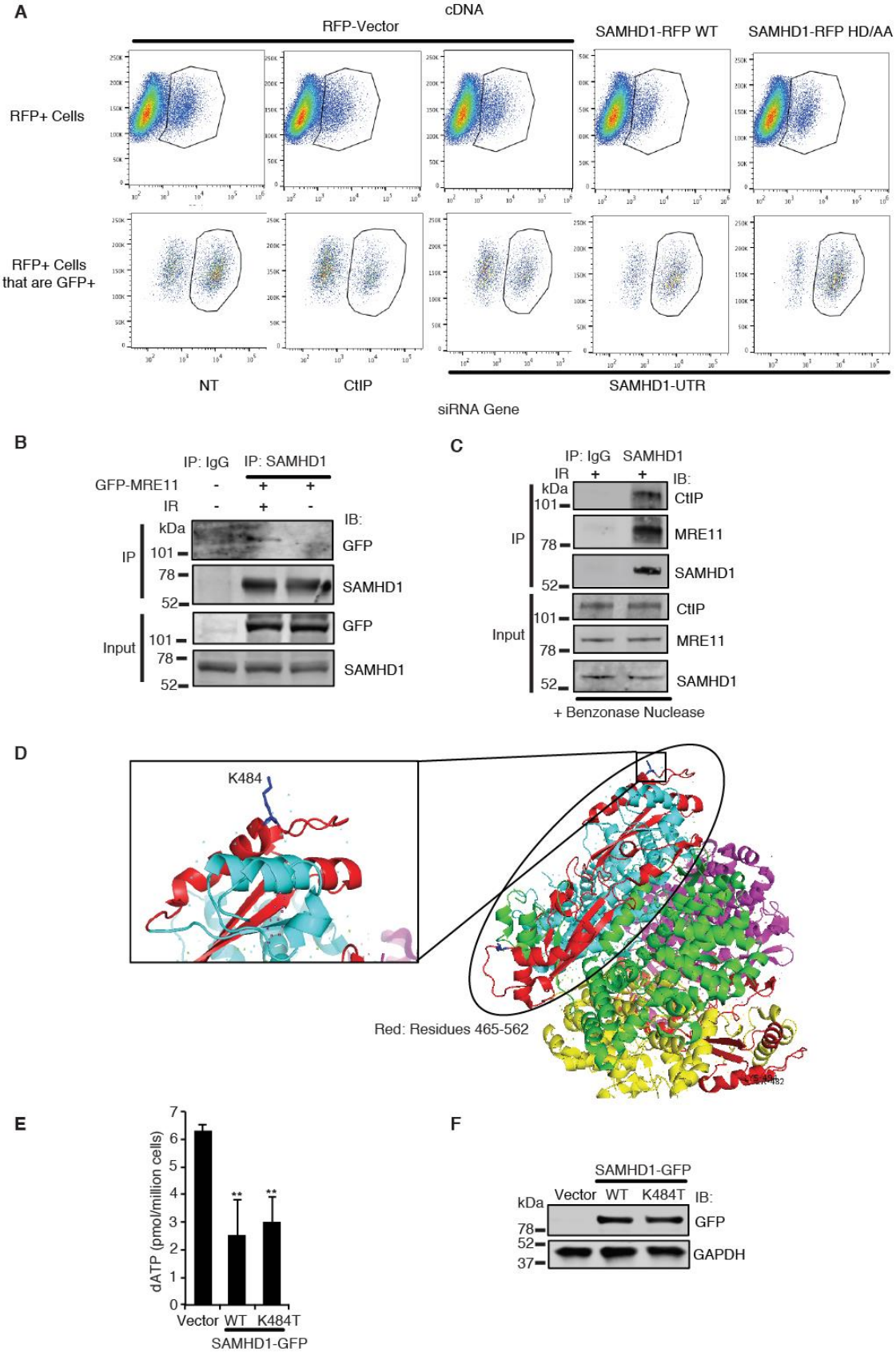
A
cDNA
RFP-Vector
SAMHD1-RFP WT
SAMHD1-RFP HD/AA
RFP+ Cells
RFP+ Cells that are GFP+
NT
CtIP
SAMHD1-UTR
siRNA Gene
B
IP: IgG
IP: SAMHD1
GFP-MRE11
IR
IB:
kDa
IP
101
78
52
GFP
SAMHD1
Input
C
IP: IgG
SAMHD1
CtIP
MRE11
+ Benzonase Nuclease
D
K484
Red: Residues 465-562
E
dATP (pmol/million cells)
Vector
WT
K484T
SAMHD1-GFP
F
SAMHD1-GFP
GAPDH
37

Figure S5 is Related to Figure 5. SAMHD1 Promotes DSB Repair by HR Independent of its dNTPase Activity and Complexes with CtIP in Response to DNA Damage. (A) U2OS cells integrated with a DR-GFP HR reporter substrate were transfected with indicated siRNAs, cDNAs, and I-SceI, and fixed. RFP positive cells were gated and analyzed for HR by GFP expression using flow cytometry. RFP+ cells and RFP+ cells that are GFP+ are gated. **(B)** Endogenous SAMHD1 was IP'd from lysate from 293T cells transfected with GFP-MRE11 and treated with or without IR, washed, separated by SDS-PAGE, and immunoblotted with anti-GFP and SAMHD1 antibodies. **(C)** Endogenous SAMHD1 was IP'd from lysate from HCT-116 cells treated with IR, washed, treated with benzonase nuclease, separated by SDS-PAGE, and immunoblotted with anti-CtIP, MRE11, and SAMHD1 antibodies. **(D)** Structural analysis of SAMHD1 CtIP interaction domain highlighted in red color. The tetrameric SAMHD1 protein structure (blue, green, purple, and yellow) was obtained from the Structural Bioinformatics (RCSB) Protein Data Bank (PDB), specifically structure 4BZB. A close-up of K484, a site of a naturally occurring gastric cancer associated SAMHD1 mutation indicates that it is located on the protein surface. **(E)** dNTP samples extracted from U2OS cells overexpressing SAMHD1-GFP WT or K484T were used to perform a RT based primer extension assay to determine dATP concentration. Mean and SEM of dATP concentration from three replicas is shown. ** $p < 0.01$. **(F)** Western blot analysis showing overexpression of SAMHD1-GFP WT and K484T in U2OS cells 72 h after transfection at which time dATP concentration was determined in **(E)**.

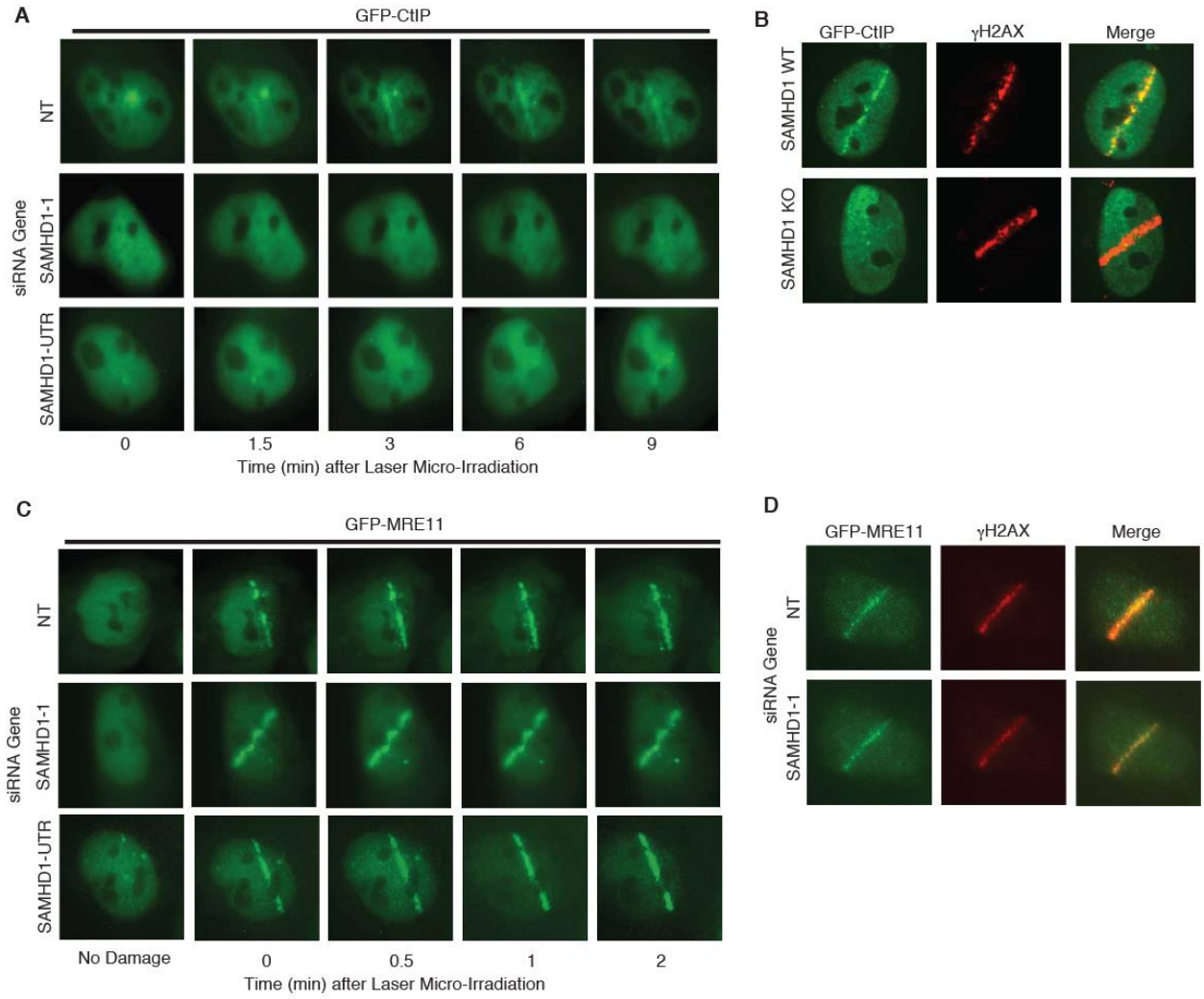

Figure S6 is Related to Figure 6. SAMHD1 Depletion Impairs CtIP but not MRE11 Recruitment to DNA Damage Sites. (A) Representative live-cell images of GFP-CtIP expressing U2OS cells transfected with NT or SAMHD1 siRNA, subjected to laser micro-irradiation, and monitored in real-time by direct immunofluorescence. **(B)** Representative images of GFP-CtIP expressing U2OS SAMHD1 WT and KO cells subjected to laser micro-irradiation, fixed 5 minutes after DNA damage, and processed for indirect immunofluorescence with anti-γH2AX antibodies. **(C)** Representative live-cell images of GFP-MRE11 expressing U2OS cells transfected with NT or SAMHD1 siRNA, subjected to laser micro-irradiation, and monitored in real-time by direct immunofluorescence. **(C)** Representative images of GFP-MRE11 expressing U2OS cells transfected with NT or SAMHD1 siRNA, subjected to laser micro-irradiation, fixed 5 minutes after DNA damage, and processed for indirect immunofluorescence with anti-γH2AX antibodies.

Figure S7 is Related to Figures 1-7. Original Uncropped Western Blots

Figure 1D - SAMHD1, GAPDH

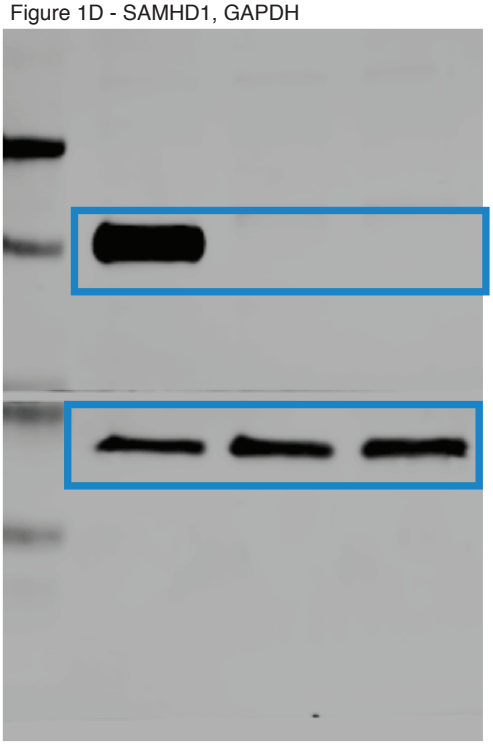

Figure 1F - GFP

Figure 1F - SAMHD1

Figure 1F - GAPDH

Figure 3H - SAMHD1

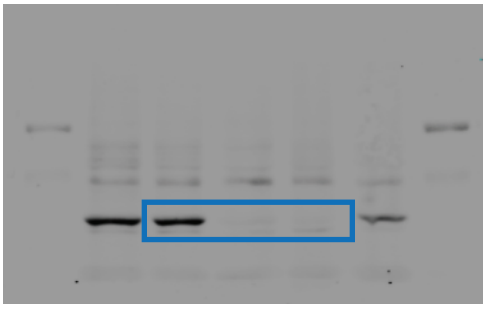

Figure 3H - GAPDH

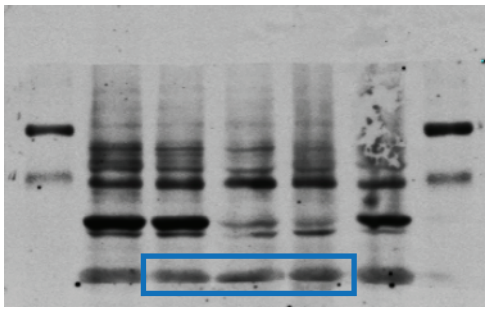

Figure 4A - SAMHD1, GAPDH

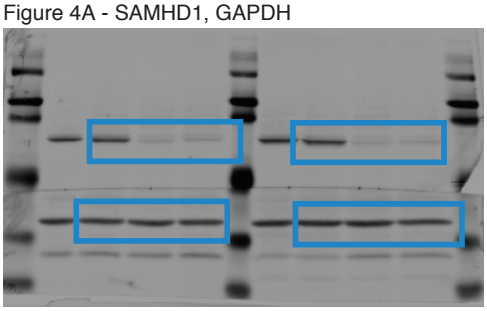

Figure 4A - pRPA32-S2/S4

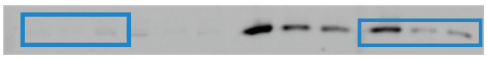

Figure 4A - RPA32

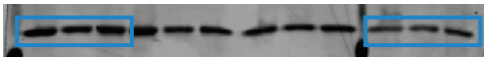

Figure 4G - p-ATR-Thr1989

Figure 4G - ATR

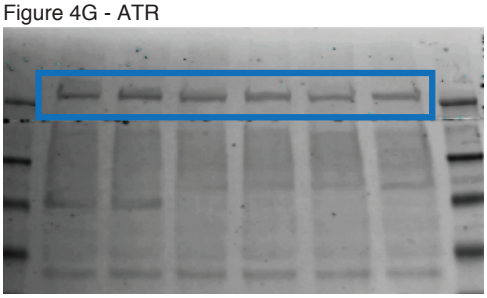

Figure 4G - SAMHD1

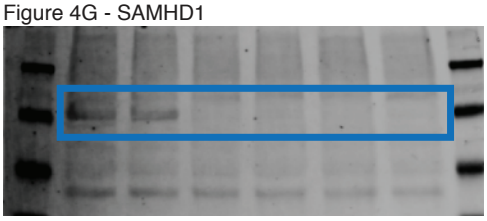

Figure 4G - GAPDH

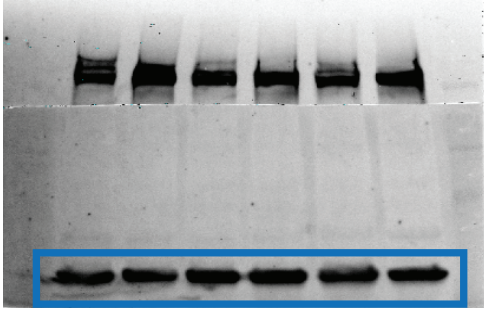

Figure 5B - SAMHD1

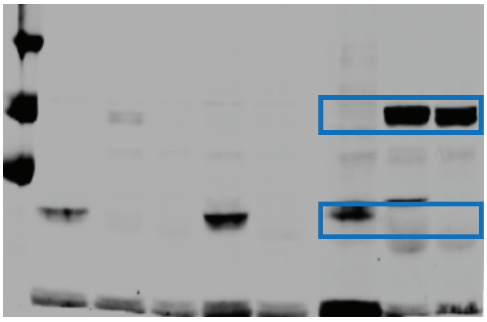

Figure 5B - GAPDH

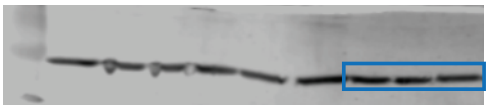

Figure 5D - IP - Input - GFP

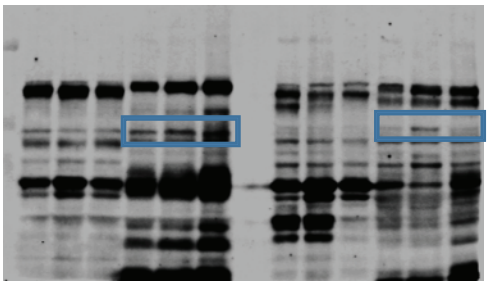

Figure 5D - IP - MRE11

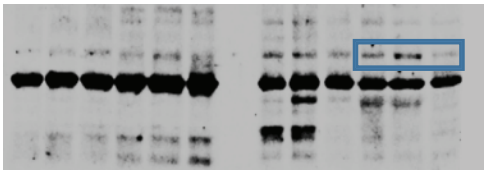

Figure 5D - IP - HA

Figure 5D - Input - MRE11

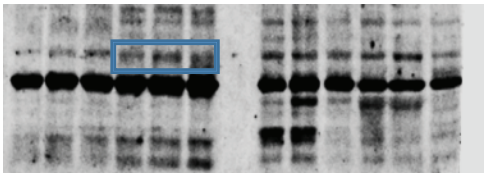

Figure 5D - Input - HA

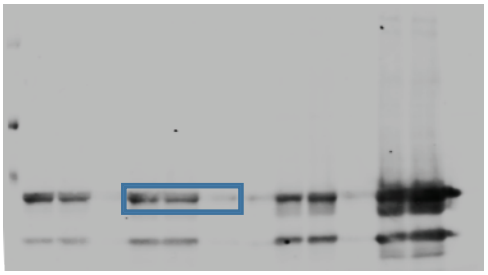

Supplemental Figure S7

Figure 5E - IP - CIP

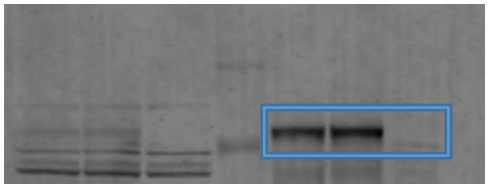

Figure 5E - IP - SAMHD1

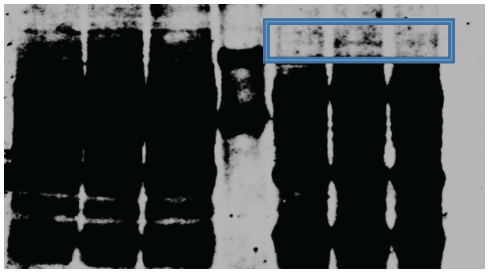

Figure 5E - Input - CIP

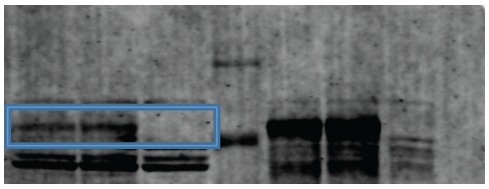

Figure 5E - Input - SAMHD1

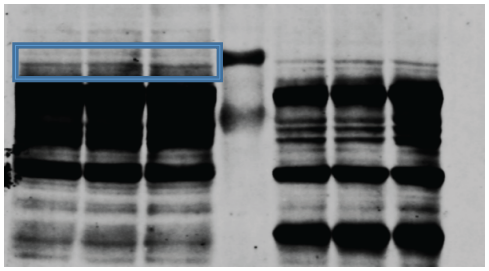

Figure 5F - IP - CIP

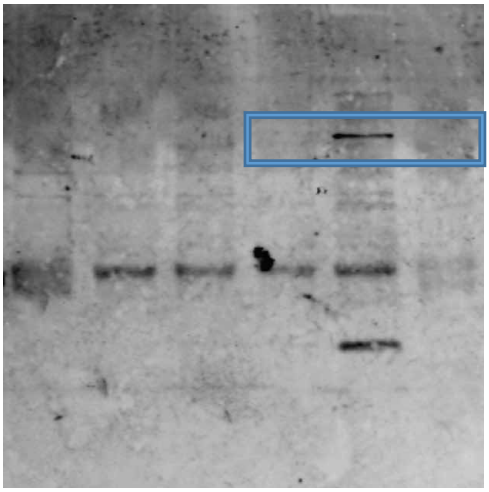

Figure 5F - IP - SAMHD1

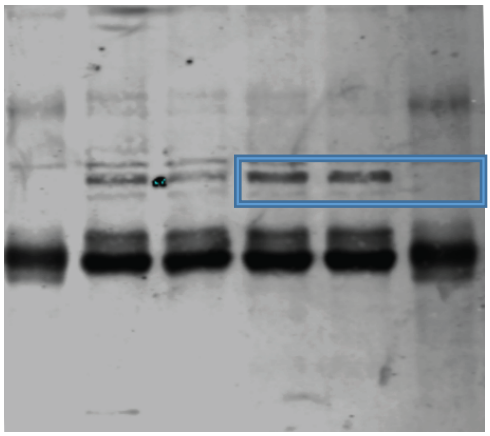

Figure 5F - Input - CtIP

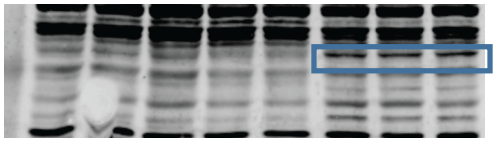

Figure 5F - Input - SAMHD1

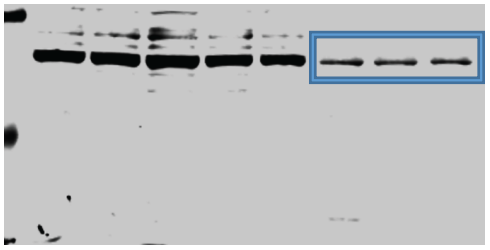

Figure 5G - SAMHD1

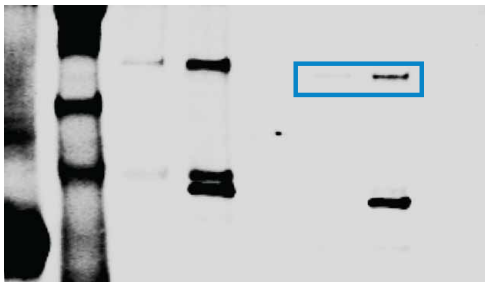

Figure 5G - CtIP

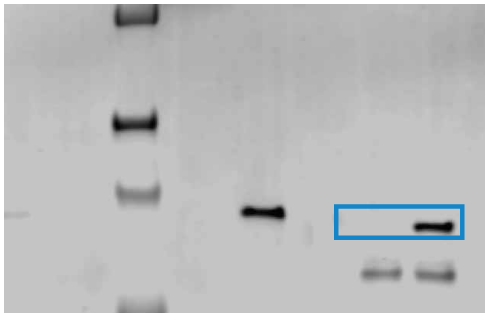

Figure 5H - IP - GFP

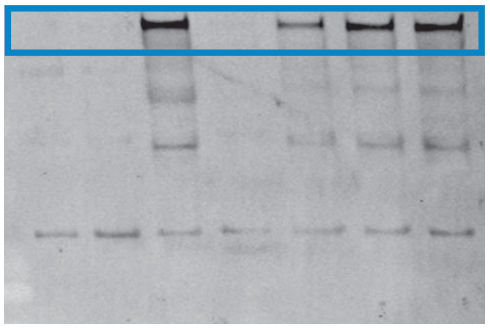

Figure 5H - IP - HA

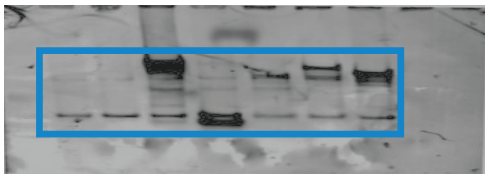

Figure 5H - Input - GFP

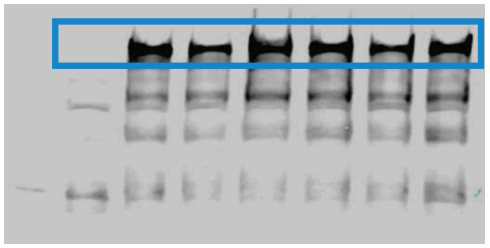

Figure 5H - Input - HA

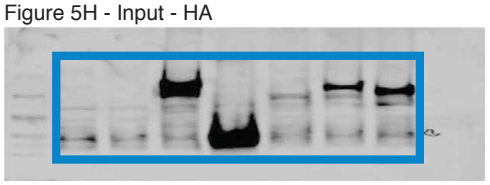

Supplemental Figure S7

Figure 5I - IP - GFP

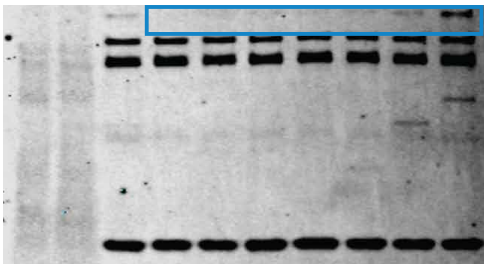

Figure 5I - IP - HA

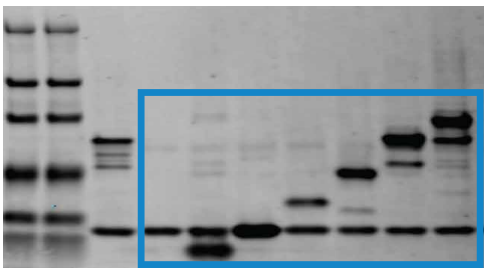

Figure 5I - Input - GFP

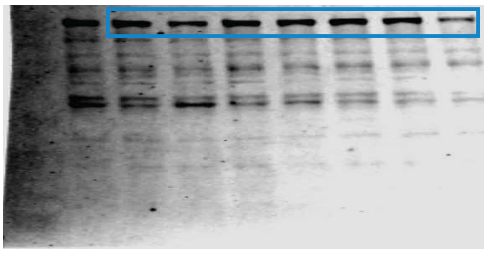

Figure 5I - Input - HA

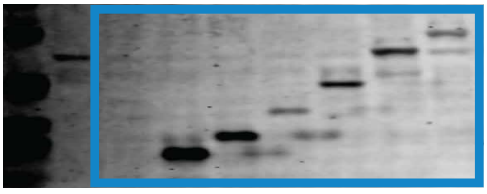

Figure 5K - IP - GFP

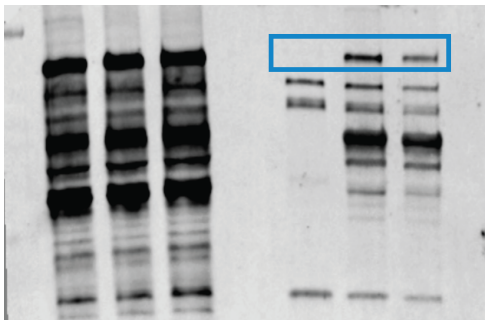

Figure 5K - IP, Input - HA

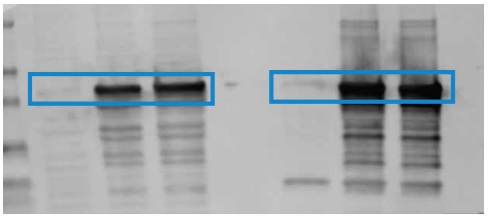

Figure 5K - Input - GFP

Figure 6F - CtIP

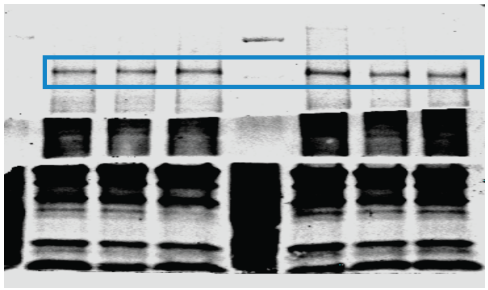

Figure 6F - SAMHD1

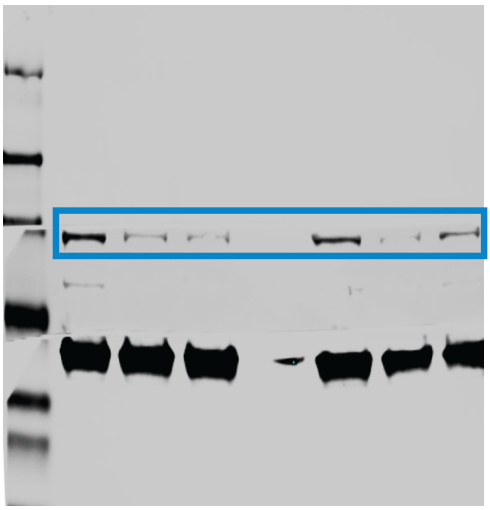

Figure 6F - NS

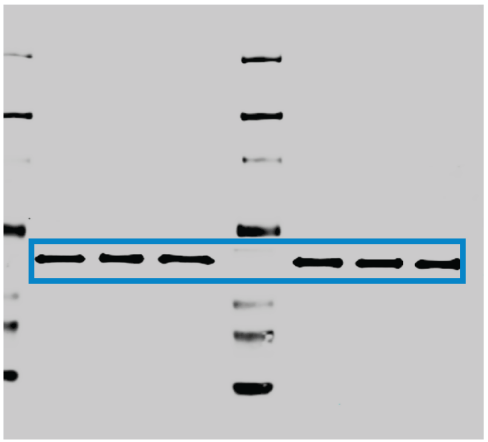

Figure 6J - SAMHD1, GAPDH

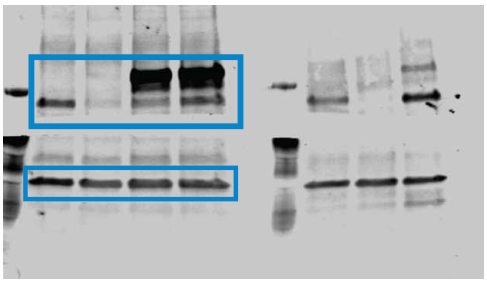

Figure 7A - SAMHD1

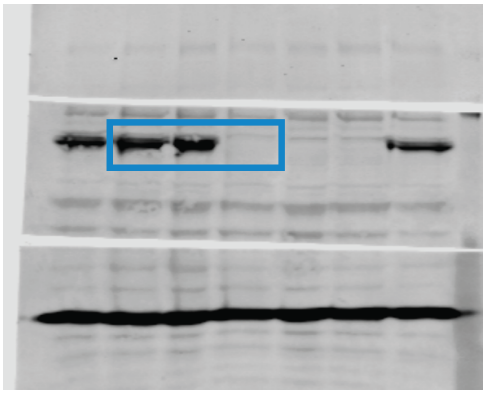

Figure 7A - GAPDH

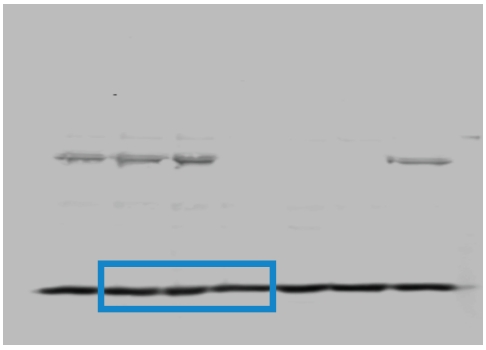

Figure 7E - SAMHD1, GAPDH

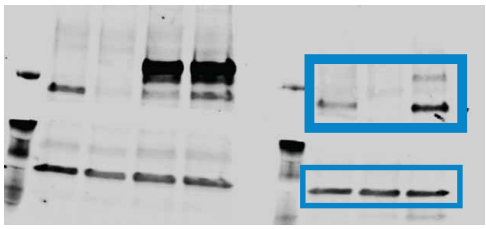

Supplemental Figure S7

Figure S1B - SAMHD1

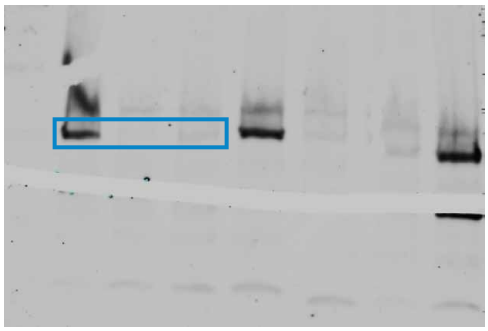

Figure S1B - GAPDH

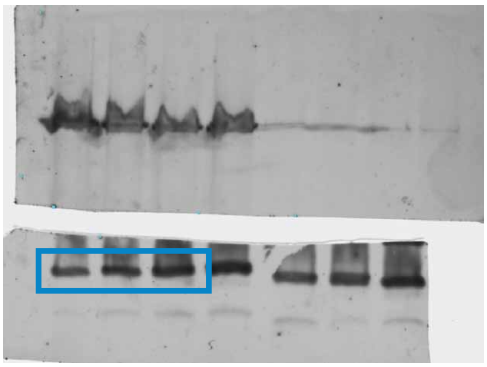

Figure S1D - SAMHD1

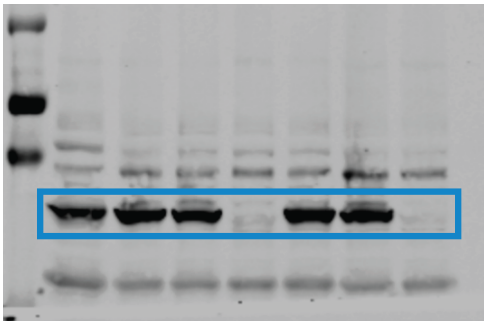

Figure S1D - GAPDH

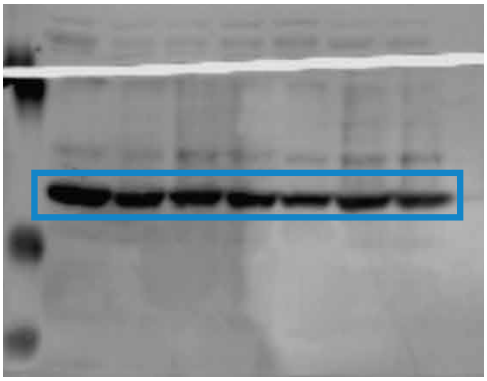

Figure S3C - SAMHD1

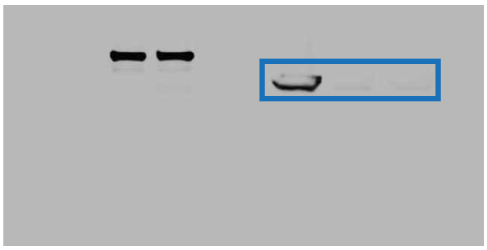

Figure S3C - GAPDH

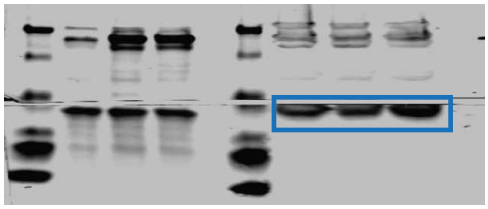

Figure S3D

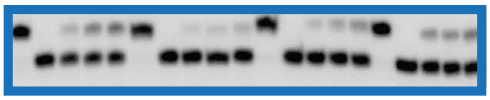

Figure S3I - SAMHD1

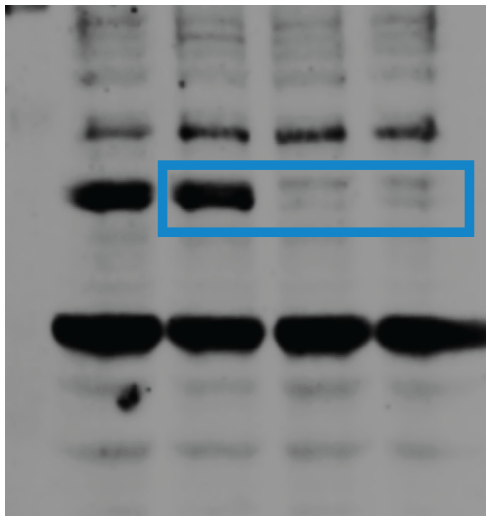

Figure S3I - GAPDH

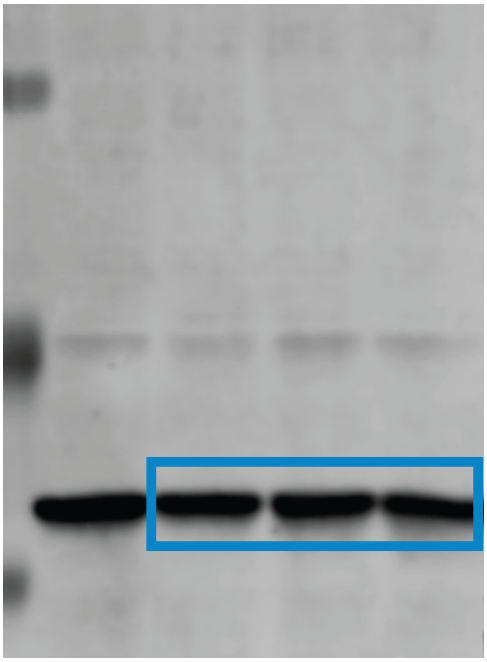

Figure S4D - SAMHD1

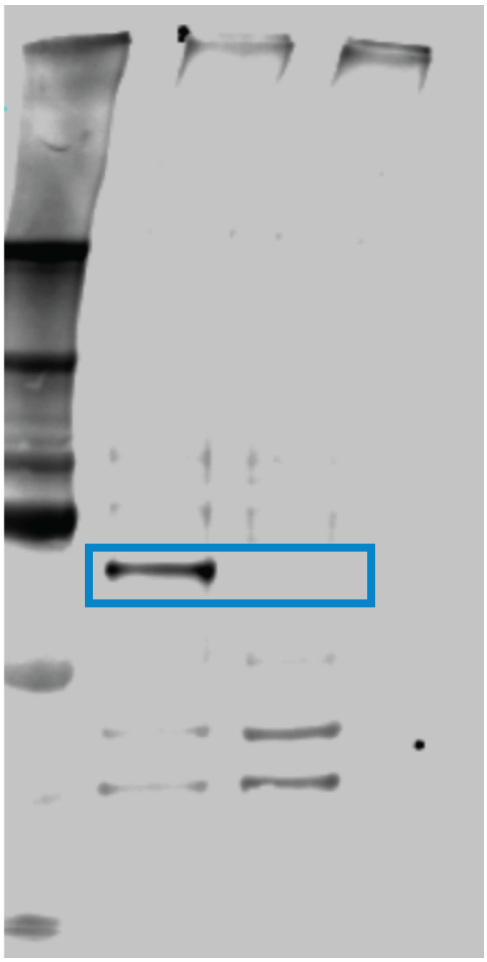

Figure S4D - GAPDH

Supplemental Figure S7

Figure S5B - IP - GFP

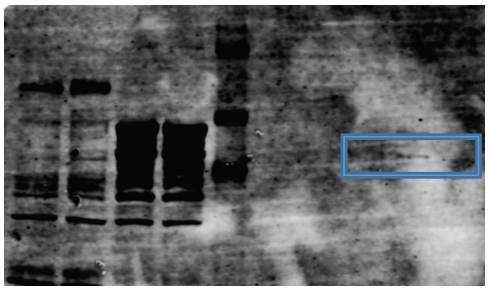

Figure S5B - IP, Input - SAMHD1

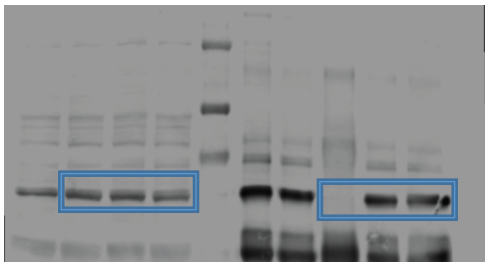

Figure S5B - Input - GFP

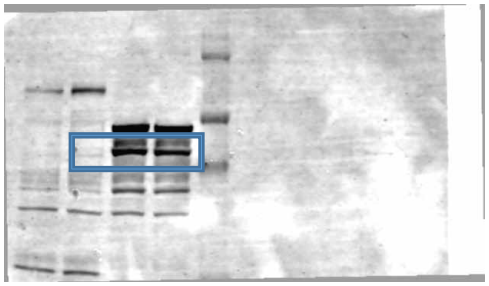

Figure S5C - IP - CtIP

Figure S5C - IP - MRE11

Figure S5C - IP - SAMHD1

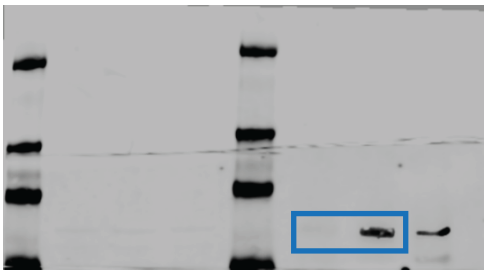

Figure S5C - Input - CtIP

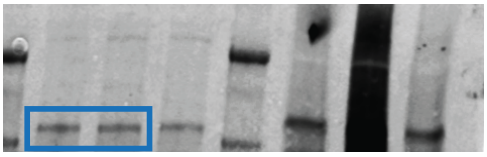

Figure S5C - Input - MRE11

Figure S5C - Input - SAMHD1

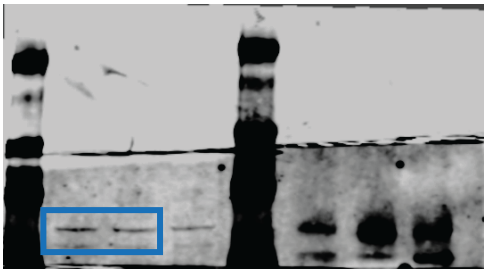

Figure S5F - GFP

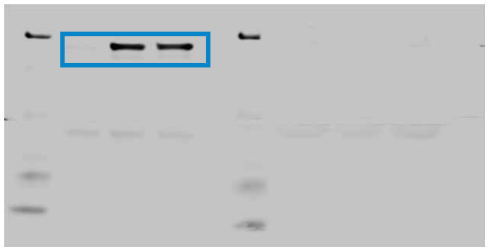

Figure S5F - GAPDH

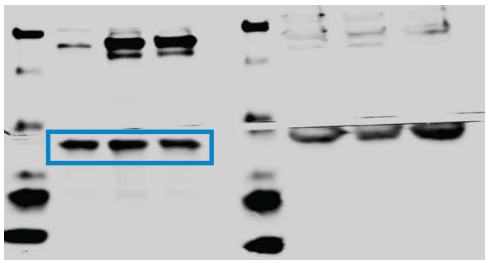

Supplemental Figure S7

SUPPLEMENTAL EXPERIMENTAL PROCEDURES

siRNA Sequences

NT (ATGAACGTGAATTGCTCAATT)
siCtIP (siCtIp-1 (GCUAAAACAGGAACGAAUC)
siSAMHD1 #1 (CAACCAGAGCUGCAGAUAA)
siSAMHD1 #2 (GAUUCAUUGUGGCCAUAUAA)
siSAMHD1 5' UTR (ACGCAUGCUGAAGCTAAGTAA)
siBRCA2 (GAGACACAAUUACAACUAAA)
siBRCA1 (CAGCAGUUUAUUACUCACUAA).

Immunoprecipitation

Cells were harvested in PBS and lysed in IP lysis buffer (0.75% CHAPS, 10% glycerol, 150 mM NaCl, 50 mM Tris pH 7.5) freshly supplemented with protease inhibitors. Lysates were centrifuged for 15 minutes at maximum speed. Supernatants were then collected, diluted by same volume of IP buffer with no CHAPS to adjust the CHAPS concentration to 0.375% and protein concentration was determined. Approximately 3-4 mg of protein were used for IP. Over expressed proteins with HA, Flag, or GFP/RFP tag were IP'd using HA agarose beads (Sigma), FLAG M2 affinity beads (Sigma), or GFP antibody (Abcam; Ab6556) and protein A agarose beads (Invitrogen) respectively, while indicated specific antibody combined with IgG was used for endogenous IP. Complexes were washed 4 times with IP buffer containing 0.375% CHAPS and protease inhibitors. IP with normal rabbit IgG or from cells that do not express epitope-tagged protein were used as negative controls. Protein/bead complex was boiled in the presence of SDS loading dye and separated by centrifugation. Supernatant containing IP'd proteins was resolved using SDS page gel as described under Immunoblot section.

Binding Assay

GST-tagged full length SAMHD1, containing a PreScission Protease site, was expressed in *E. coli* and purified using glutathione-Sepharose as described previously (Hollenbaugh et al., 2017). GST tag was removed post purification by incubating with precision protease. GST-tagged CtIP was purchased from Novus. Recombinant proteins (GST-CtIP + no SAMHD1, or GST-CtIP + SAMHD1) were precleared with protein A agarose beads (Invitrogen). The complex was washed and incubated overnight with anti-SAMHD1 antibody (Origene, TA502024) and protein A beads (Invitrogen) in IP buffer with .375% Chaps, described above. The beads were washed with IP buffer, boiled in presence of SDS loading dye and resolved on SDS page gel as described under Immunoblot section. The interacting profile was visualized after staining with anti-SAMHD1 and CtIP antibodies (kind gift from Dr. Richard Bear)

Immunofluorescence Analysis

U2OS, HeLa, BEAS-2B, or small airway epithelial cells were seeded on coverslips were treated with 3 μM CPT or 10 Gy of IR. After the indicated recovery time, cells were fixed with 4% (wt/vol) paraformaldehyde (EMD Chemicals) for 10 minutes at room temperature, permeabilized with 0.5% Triton X-100 (Fisher Scientific) for 10 minutes, and then blocked with 5% BSA in PBS. Cells were immunostained with indicated primary antibody diluted in 1% BSA, followed by Alexa Fluor 488, 555, or 647 anti-rabbit/mouse secondary antibody (Life technology) diluted in 1% BSA in PBS. Coverslips were mounted with DAPI Fluoromount-G (Southern Biotech) on slides and images were captured using a 63x oil objective on a Zeiss Observer Z1 microscope equipped with Axiovision Rel 4.8 software. The percentage of cells with indicated foci was counted from three replicate experiments with at least 50 cells counted per replicate. Unless specified otherwise γH2AX induction was used as control for damaged cells and cells containing greater than five foci were counted.

Clonogenic Assay

U2OS or MCF-7 cells were plated at a density of $3x10^2$ cells/well in 6 well plates 24 hours after siRNA knockdown. Plating efficiency following siRNA knockdown was greater than 95%. Cells were allowed to adhere for 24 hours after plating, and then drug treated or irradiated at doses as indicated. Cell media was changed 24 hours post-irradiation or drug treatment, and every 5 days thereafter. Cells were allowed to proliferate and methanol fixed and stained with crystal violet reagent after 10-14 days. Colonies containing greater than 50 cells were manually counted and total numbers of cells at each radiation dose were normalized to non-treated control.

DSB Repair Reporter Assay

To determine HR-mediated DSB repair efficiency cells U2OS stably expressing DR-GFP reporter gene, described previously (Pierce et al., 1999), were transfected with 30 nM siRNA using Liptofectamine RNAiMax

(Invitrogen). The following day, media was changed and cells were transfected with plasmids (I-SceI and RFP). 72hrs post plasmid transfection, cells were harvested and fixed in 1% PFA for FACS analysis. Cells expressing RFP were gated and analyzed for HR efficiency based on GFP expression. For rescue assays, I-SceI was co-transfected with RFP or SAMHD1-RFP (WT or HD/AA). To determine NHEJ-mediated DSB repair efficiency, we utilized a reporter gene based assay previously described (Seluanov et al., 2004). Briefly, pEGFP-Pem1-Ad2 was digested with I-SceI and gel purified to ensure the homogeneity of digested population. U2OS cells were transfected with non-targeting and two independent SAMHD1 siRNA while one group was treated with NU7206, a DNA-PKcs inhibitor. The next day, media was changed and cells were transfected with I-SceI digested pEGFP-Pem1-Ad2. DNA-PKCs inhibitor was kept on throughout the experiment. Cells were harvested and fixed in 1% PFA for GFP expression analysis by FACS. For the rescue assay, RFP positive cells were gated and analyzed for HR efficiency using GFP expression as readout.

Laser Microirradiation Assay

U2OS SAMHD1 WT or KO cells were transfected with GFP-RPA70, GFP-CtIP, GFP-MRE11, or SAMHD1-GFP/RFP WT or K484T. 15 hours post transfection, media was changed and cells were left to grow or plated for siRNA transfection. For SAMHD1 depletion induced impairment of RPA70 or CtIP, cells were transfected with indicated siRNA 24 hours post plasmid transfection. 48 hours post siRNA transfection, cells were plated on 35-mm glass bottom dishes (MatTek Corporation) for laser microirradiation. Laser microirradiation was performed on a Zeiss Observer Z1 microscope equipped with a Micropoint® Laser Illumination and Ablation System (Photonic Instruments). The laser output was set to 80 %, which can reproducibly give a focused GFP-RPA70 stripes. The GFP or RFP stripes were recorded at indicated time points and then analyzed with ImageStudiolite. For assays involving endogenous proteins, localization to laser site was analyzed by subjecting cells to microirradiation, fixed in 4% PFA and visualized as indicated under the immunofluorescence assay described above.

DNA End Resection

To determine DNA end resection, U2OS, BEAS-2B, or small airway epithelial cells depleted of SAMHD1 using two independent siRNA or U2OS SAMHD1 WT and KO cells were treated with CPT for 4 hours, 72 hours post transfection. Then cells were fixed in 4% PFA and analyzed for γH2AX and RPA70 foci. For BrdU foci dependent DNA end resection analysis, cells were depleted of SAMHD1 and incubated with 30 μM BrdU for 36 hours and then treated with 3 μM CPT for 4 hours. Then cells were fixed following pre-extraction. Briefly, cells were washed with cytoskeleton buffer (CSK) (10 mM PIPES, 300 mM Sucrose, 100 mM NaCl, 3 mM $MgCl_2$, 1mM EGTA) and incubated in extraction buffer (0.5% Triton X100 in CSK buffer) at room temperature on a rocker for 15 min. Then cells were washed with PBS, fixed and processed as described in the immunofluorescence assay section. For both RPA70 and BrdU foci based assays, fifty cells possessing γH2AX foci were counted three times independently and RPA or BrdU foci was compared between SAMHD1 depleted and non-depleted cells.

Comet Assay

U2OS cells were depleted of SAMHD1 or CtIP using siRNA as described above. 48 hours post-transfection and following 20 hours incubation with 500 μM mimosine, cells were released for 7 hours and embedded in 0.5% low melting point agarose (Lonza) on individual slides. Then some of the slides were exposed to 10 Gy IR and then incubated in complete media to allow for repair. At the indicated time, the cells were lysed for 2 hours in 10 mM Tris, pH 10, 2.5M NaCl, 10 mM EDTA, 1% Triton X-100 and 10% DMSO at 4ºC. Lysis buffer was exchanged for TBE (220 mM Tris, 180 mM Borate, 5 mM EDTA pH 8.3) with three 10 minutes incubations. Electrophoresis was conducted at 20V for 30 min in TBE and cells were stained with sybr green (Invitrogen). At least ten fields per slide where photographed at random by direct fluorescence microscopy using an Olympus IX81 epifluorescence microscope. Fifty comets per slide were scored employing CometScore Software (TriTek). Dot plot graphs were generated with KaleidaGraph 4.5.2. Statistical analysis was performed using a Wilcoxon signed-rank test.

Cellular dNTP Pool Quantification

Cellular dNTP pool was measured as described previously (Lahouassa et al., 2012). Briefly, cells were depleted of SAMHD1 by transfecting with two different siRNAs or transfected with SAMHD1-GFP WT or K484T. 72 hours post transfection, cells were washed with cold PBS and were lysed in 65% aqueous methanol. Lysates were heated to 95 °C, cleared by centrifugation, dried and resuspended in water. An 18-nucleotide primer labeled at the 5′ end with ^{32}P was annealed to four different 19-nucleotide templates creating nucleotide variation at the 5′ end of the

template. The cell extracts were used as dNTP source to extend a single nucleotide at the 5' end of the primer. Extended and unextended products were resolved on urea-PAGE and analyzed. The frequency of extended primers was determined with QuantityOne software. Dilutions required to obtain extension with in linear range was determined for each sample and used to perform the assay.

Knock Out cells Generation

The guide RNA (gRNA) sequences cloned in to All-in-one Cas9 and gRNA expression plasmid were purchased from Sigma. Two unique gRNAs targeting the 4th (gRNA1 CCTCGTCCGAATCATTGATACA) or 6th exon (gRNA2 TGCTCGCCCGGAGGTGAAATGG.) of SAMHD1 were selected in consultation with Sigma. HCT-116 and U2OS cells were transfected with all-in-one plasmid expressing cas9, SAMHD1-targeting gRNA, and GFP. 48 hours post-transfection, GFP-positive cells were sorted and plated and seeded in 96-well plates, one cell per well. Cells were grown for three weeks and analyzed for SAMHD1 expression as compared to WT and two colonies exhibiting SAMHD1 knockout were used for analysis.

Chromatin Fractionation Assay

HCT-116 cells were treated with 10 Gy IR and harvested after 1 hour recovery. Cells were trypsinized, washed with ice-cold PBS and fractionated as described previously (Mendez and Stillman, 2000). Briefly cells were lysed in buffer A (10mM HEPES, 10mM KCL, 1.5mM MgCl2, 0.34 M sucrose, 10% Glycerol, 1mM DTT and protease inhibitors) and incubated on ice for 5 minutes. The lysate was centrifuged and the pellet was washed with Buffer B (3mM EDTA, 0.2 mM EGTA, 1mM DTT and protease inhibitors). The lysate was then resuspended in 50% Buffer A/ B, boiled in presence of SDS, and sonicated. The samples were resolved on SDS-PAGE and visualized with the Licor Odyssey system.

Super Resolution Imaging

U2OS cells (ATCC HTB-96) were grown in McCoy's 5A (Modified) medium (ThermoFisher 16600) with 10% FBS (Gemini Bio. 100-106) and 100 U/mL Penicillin-Streptomycin (ThermoFisher 15140). Cells were seeded on glass coverslips for 24 hours prior to 72 hours culture in FBS free medium to achieve a G0/G1 phase synchronization. Release back into full medium for 16 hours produced a mid-S phase cell population. To induce one-sided DSBs cells were treated with 100 nM CPT (Abcam 120115) for 1 hour. Simultaneously, naDNA was pulse-labeled with 10 μM EdU (Click-iT kit, ThermoFisher C10340). Cells were allowed to recover from CPT damage for a further hour prior to pre-extraction in room temperature CSK buffer (10 mM Hepes, 300 mM Sucrose, 100 mM NaCl, 3 mM $MgCl_2$, and 0.5% Triton X-100, pH = 7.4) for 2-3 minutes followed by fixation for 15 minutes in paraformaldehyde (3.7% from 32% EM grade, Electron Microscopy Sciences, 15714) and glutaraldehyde (0.3% from 70% EM grade, Sigma-Aldrich, G7776) in PBS. For Alexa Fluor 647 fluorescent labeling of the nascent DNA, the copper catalyzed 'Click' reaction was used as described in the Click-iT protocol (ThermoFisher, C10640). The cells were blocked with blocking buffer (2% glycine, 2% BSA, 0.2% gelatin, and 50 mM NH_4Cl in PBS) for 1 hour at room temperature (RT) and then immunostained in for SAMHD1 (mouse monoclonal, Origene TA502024) and CtIP (rabbit polyclonal, Santa Cruz, sc22838) with Alexa Fluors 568 and 488 secondary antibodies (Life Science).

Prior to imaging, coverslips were mounted in SR buffer containing 1 mg/mL glucose oxidase (SigmaAldrich, G2133), 0.02 mg/mL catalase (SigmaAldrich, C3155), 10% glucose (SigmaAldrich, G8270)) and 100 mM mercaptoethylamine (Fisher Scientific, BP2664100) in PBS. S-phase cells were then identified by strong EdU signal and imaged sequentially for three-color detection using a custom-built SR microscope based on a Leica DMI 3000 inverted microscope. Briefly, 488 nm (Coherent, 87-461, 150 mW), 556 nm (UltraLasers, MGL-FN-556 200 mW) and 640 nm (OEM Laser Systems, MLL-III 150 mW) laser lines were combined using appropriate dichroics and focused onto the back aperture of a HCX PL APO 60X NA = 1.47 TIRF (Leica) objective via a multi-band dichroic (Chroma, UF1C165837). For each area of interest 2000 sequential frames of single molecule emissions at 40 Hz were collected through the same objective and dichroic and imaged on a Prime 75B CMOS camera (Photometrics) using MicroManager.

Each raw image stack was processed for single molecule localization and rendered using 20 nm pixels via rapidSTORM. These images were then mapped to correct for chromatic aberrations using Tetraspecks (beads were acquired across all three colors (Tetraspecks, 100 nm) as a reference sample and an elastic transformation generated using bUnwarpJ in FIJI. To determine the degree of colocalization in the resulting, thresholded (Otzu) three-color images, Monte Carlo simulations were used to randomly rearrange the clusters within an ROI to calculate a baseline level of random colocalization. Using this approach, 20 random simulations were generated for each nucleus in a pair-wise fashion, examining Red/Green, Red/Blue, and Green/Blue overlap. The total number of overlaps detected in each nucleus (typically 15-100) could then be normalized to the determined random level of overlap by dividing the number of real overlaps by the average number of overlaps in the same randomly-simulated nucleus. We display

these values as the normalized colocalization level above random where random overlap has a value of 1. For display purposes, images were smoothed by applying a Gaussian blur filter and colors were thresholded to best produce a clear picture of the single foci.

Experiments were carried out in triplicate with between 10 and 25 nuclei imaged for each sample. Nuclei were excluded based on poor image quality (non-S-phase, aggregated fluorophores) or very low numbers of clusters in any color (<10). Between 31 and 75 nuclei were used to generate the data. A student's t-test was used to test for significance of difference between means of control and damaged samples with ** denoting $p<0.01$ and **** denoting $p<0.0001$.

Statistical Analysis

Unless otherwise stated, all experiments were performed at least three times. Results were analyzed using unpaired two-tailed Student's t test and data expressed as mean ± SEM. p values less than 0.05 were considered statistically significant.

SUPPLEMENTAL REFERENCES

Mendez, J., and Stillman, B. (2000). Chromatin association of human origin recognition complex, cdc6, and minichromosome maintenance proteins during the cell cycle: assembly of prereplication complexes in late mitosis. Molecular and cellular biology *20*, 8602-8612.